

# Spatiotemporal Learning of Multivehicle Interaction Patterns in Lane-Change Scenarios

Chengyuan Zhang, *Student Member, IEEE*, Jiacheng Zhu, Wenshuo Wang, *Member, IEEE*, Junqiang Xi

**Abstract**—Interpretation of common-yet-challenging interaction scenarios can benefit well-founded decisions for autonomous vehicles. Previous research achieved this using their prior knowledge of specific scenarios with predefined models, which limits their adaptive capabilities. This paper describes a Bayesian nonparametric approach that leverages continuous (i.e., Gaussian processes) and discrete (i.e., Dirichlet processes) stochastic processes to reveal underlying interaction patterns of the ego vehicle with other nearby vehicles. Our model relaxes dependency on the number of surrounding vehicles by developing an acceleration-sensitive velocity field based on Gaussian processes. The experiment results demonstrate that the velocity field can represent the *spatial* interactions between the ego vehicle and its surroundings. Then, a discrete Bayesian nonparametric model, integrating Dirichlet processes and hidden Markov models, is developed to learn the interaction patterns over the *temporal* space by segmenting and clustering the sequential interaction data into interpretable granular patterns automatically. We then evaluate our approach in the highway lane-change scenarios using the highD dataset, which was collected from real-world settings. Results demonstrate that our proposed Bayesian nonparametric approach provides an insight into the complicated lane-change interactions of the ego vehicle with multiple surrounding traffic participants based on the interpretable interaction patterns and their transition properties in temporal relationships. Our proposed approach sheds light on efficiently analyzing other kinds of multi-agent interactions, such as vehicle-pedestrian interactions.

**Index Terms**—Multi-vehicle interaction, lane-change scenarios, Gaussian velocity field, Bayesian nonparametrics.

## I. INTRODUCTION

CHANGING lanes in complex and diverse scenarios has become stubborn bottlenecks in the safe deployment of autonomous vehicles due to the uncertainty in the way of nearby human-related agents behave [1], [2]. Human drivers can react to fast-varying surrounding traffics adaptively during changing lanes according to their perception and experiences but could not exhaustively enumerate explicit rules and models for all scenarios from collected raw data solely as the flood of data can overwhelm human insight and analysis [3]. This is one of the core reasons why the specific models designed according to prior knowledge for autonomous vehicles can not deal with the entire scenarios encountered in the real world.

(Corresponding authors: Wenshuo Wang)

C. Zhang is with the Department of Mechanical Engineering, University of California, Berkeley (UCB), CA, USA, 94720. (e-mail: enzozcy@gmail.com).

J. Zhu is with the Department of Mechanical Engineering, Carnegie Mellon University, Pittsburgh, PA, USA, 15213. (e-mail: jzhu4@andrew.cmu.edu).

W. Wang is with the California Partners for Advanced Transportation Technology (PATH), UC Berkeley, USA. (e-mail: wwsbit@gmail.com).

J. Xi is with the Department of Mechanical Engineering, Beijing Institute of Technology, Beijing, China. (e-mail: xijunqiang@bit.edu.cn).

Some research designs tailored decision-making policies for a specific circumstance under strong assumptions [4], [5], for example, only considering the nearest vehicles, which would make behavior modeling and controller design much more feasible. For instance, Zhou *et al.* [4] assumed that only the nearest surrounding vehicles on the target lane have an impact on decision-making and would always agree to leave a merge-in space, thus allowing the ego vehicle to merge. However, they are far away from the real-world cases in which human driver usually makes decisions according to their comprehensive evaluation of surroundings in a specific spatiotemporal range [6].

Researchers have developed several advanced machine learning techniques to model the interaction between the ego vehicle and its surroundings, as well as infer lane-change intents. However, most of these techniques are only suitable for the limited scenarios with the fixed number of nearby vehicles or with only considering the nearest vehicles. For example, the Bayesian networks in [7], [8] required well-structured road conditions and only considered the nearest well-observed vehicles. Similar limitations exist in the game theory of modeling multi-agent interactions [6]. On the contrary, in real world, human drivers would comprehensively consider the entire scenario information within a region of interest (ROI) to make a proper decision, rather than only using the information of the nearest vehicles [9]. However, the number of vehicles in the ROI is ordinarily changing over time, which brings significant challenges in modeling the interaction behaviors.

On the other hand, analysis of interaction patterns in lane-change scenarios can help researchers design associated decision-making policies and facilitate to reveal the mechanism of changing lanes. However, there is still no unified specific rule of doing pattern analysis for lane-change interaction behavior. Some researchers prefer the grid-based method over the *spatial* space in which a preset occupancy grid describes the surrounding space around the ego vehicle [8], [10], but it fails to characterize the behavioral sequences over time. Some other works use the segment-based method over the *temporal* space in which several manually predefined stages over time describe the entire lane-change behavior [1]. However, it only focused on the maneuvers/trajectories of the ego vehicle while ignoring the interaction with other vehicles. Besides, both of the above ways are subjectively defined by researchers based on their prior knowledge and tailored applications. Therefore, given a bunch of lane-change scenarios in the real world, it is not yet entirely clear “*how does the ego vehicle interact with surrounding vehicles over time in a specific space domain?*” and “*how many interaction patterns exist?*”

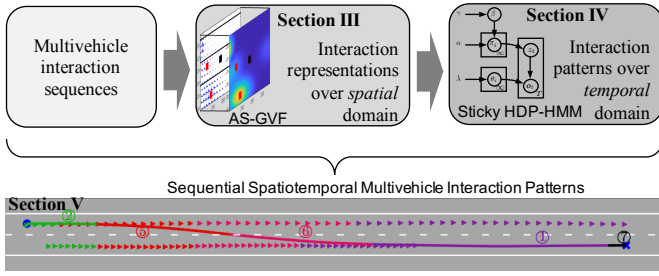


Fig. 1. The framework of learning spatiotemporal interaction patterns during lane-change scenarios.

Motivated by the above two questions, in this paper, we aim at developing an unsupervised learning framework (see Fig.1) to figure out the underlying lane-change interaction patterns for potential decision-making applications. Toward this end, we will overcome two key challenges in

- Learning representation. The representation should capture the interactions of the ego vehicle with the nearby traffic agents while being insensitive to the number of agents in the environment.
- Extracting interpretable interaction patterns. The number of patterns should increase adaptively when new scenarios are incrementally available.

Our main contributions are threefold:

- 1) Proposing a general framework that leverages continuous and discrete stochastic processes to learn and recognize the lane-change interactions of the ego vehicle with its surrounding traffics on highways.
- 2) Developing an acceleration-sensitive Gaussian velocity field to capture the interactions of the ego vehicle with its surrounding traffics in the *spatial* space while reflecting the intent of human drivers. The dimensions of this field are invariant to the number of vehicles in the environment.
- 3) Introducing a nonparametric approach to learn interaction patterns in the *temporal* space automatically without any prior knowledge of the number of underlying patterns.

The remainder of this paper is organized as follows. Section II reviews the related state-of-the-art. Section III introduces the representation learning of multi-vehicle interactions. Section IV describes the methodology (i.e., Bayesian nonparametric learning) to extract interaction patterns, and Section V explicitly analyzes the experimental results. Finally, conclusions are presented in Section VI.

## II. RELATED WORKS

### A. Lane-Change Behavior Analysis

For driving behavior analysis and classification, there is no unified framework and theory to achieve them. The required methods and features rely on research motivations such as controller design and decision-making. For instance, Woo, *et al.* [11] defined four intentions (i.e., keeping, changing, arrival, and adjustment) to represent the procedure of changing lanes based on the distance from the center line, the lateral velocity, and the potential feature. Yang, *et al.* [12] grouped the decision-making data into three driving styles - moderate,

vague, and aggressive – using the relative information between the ego vehicle and the target vehicle. Liu, *et al.* [13] classified the driving maneuvers into moving forward, turning left, and changing lane for abnormal behavior detection based on the basic dynamic and kinematic states of the target vehicles. The above behavioral categories were defined subjectively, which requires prior knowledge of different kinds of lane-change behaviors. However, the prior knowledge is diverse over data analysts. By classifying the relative trajectories, Deo, *et al.* [14] empirically defined ten maneuver classes for freeway traffic, including four lane pass maneuvers, two overtake maneuvers, two cut-in maneuvers and two drifting-into-ego-lane maneuvers, while Claussmann, *et al.* [15] distinguished them into eight common driving situations. Moreover, Do, *et al.* [10] segmented lane-change maneuvers of the ego vehicle into two stages over temporal space, and then listed 32 occupancy grid states of right lane-change over spatial space, and finally grouped them into four categories. However, they assumed that the traffic agents on its left (right) neighboring lane would not impact the right (left) lane-change behavior. By using the manually-predefined prior knowledge, Li, *et al.* [16] categorized lane change into nine driving actions based on GPS/IMU data and eight driving intentions based on front-view videos.

The above discussion concludes that manually setting a reasonable number of clusters of behavioral interactions from real-world traffic data and then tagging these clusters is a tricky problem. Even if the number of clusters is already subjectively determined according to some specific semantic settings, the unsupervised clustering results may not always match the semantic information of the prior setting [17]. Our developed model aims at adaptively learning the lane-change interaction patterns of the ego vehicle with surrounding vehicles, but it does not need prior knowledge of the number of patterns.

### B. Representation Learning for Multi-Vehicle Interactions

Representation construction for multi-vehicle interactions at each moment is critical to task performance but challenging due to the behavioral uncertainty in surrounding human-related agents. Human drivers can make decisions in complex, multidimensional environments easily and efficiently because of the powerful capability to abstract representations of the environment [18]. To retrieve useful information from environments and make proper decisions for changing lanes while interacting with other vehicles efficiently, a variety of representatives were selected in state-of-the-art such as relative distance/speed/acceleration between the ego vehicle and the target vehicle [12]. Besides, the deviations from lane center and lateral and longitudinal velocity were also adopted in [19]. Moreover, the binary-state occupancy cells attached to the ego vehicle were used to represent surrounding scenarios [7], [10]. Some works were trying to figure out the influence of feature selection on lane change behaviors in terms of behavior recognition and decision-making, thus offering cues of selecting and constructing efficient features [20], [21]. The features mentioned above and their combinations can be directly measured using sensors; however, the dimension of

all these selected features is sensitive to the number of traffic agents in the environment.

To make problem formulation tractable, researchers would classify the environment into several typical groups according to the number of involved vehicles and then select associated features subjectively. Lienke, *et al.* [19] and Wang, *et al.* [22] limited the number of surrounding vehicles to six and five, respectively, which fails to handle the situations where the number is changing over time. Hu, *et al.* [23] used the features of the closest three vehicles around the ego vehicle to predict vehicle motion and intention, but the closest vehicles may be different at other timestamps, thus causing discontinuity of some features such as the relative positions.

Potential fields, as widely selected features, have attracted many research interest in modeling multi-agent traffic scenarios due to its powerful capability to embrace different traffic factors friendly such as the types of road users, obstacles, and traffic regulations. Several kinds of potential fields have been developed for specific applications. For example, researchers in [24], [25] developed an artificial potential field, which consists of different factors such as lane marker, road condition, and vehicle states. In [26], a potential field integrated with vehicle dynamics was proposed to build a safe, robust path-planning controller for autonomous vehicles. Woo, *et al.* developed [27] a dynamic potential field, which is adaptable to the number of adjacent vehicles, to predict lane change behavior. The driving safety field of describing driver-vehicle-road interactions was also proposed for collision warning [28]. More historical developments of field-relevant features refer to the review work [15]. Here, we will develop a novel potential field based Gaussian processes, which can consider a varying number of surrounding vehicles while capturing the dynamic interactions among multiple vehicles and the motion trends of each surrounding vehicle. More details will be provided in Section III.

### C. Bayesian Nonparametrics for Driving Behavior

Chopping complex sequential behavior into small segments and clustering them into groups helps us gain an insight into what happens inside it. Setting a reasonable number of clusters is always tricky in conventional clustering algorithms such as  $k$ -means and Gaussian mixture models (GMM) [29]. It requires trial and error to get satisfied [30]. Instead of treating the number of components and clusters as a constant, Bayesian nonparametric models treat it as a random variable by adding a functional distribution layer; for example, by adding a Dirichlet process to GMM [31], [32]. Bayesian nonparametrics has demonstrated its powerful ability to model and predict dynamic processes with the number of patterns a priori unknown [33]–[35].

In driving behavior analysis and prediction, the Bayesian nonparametric models have also been implemented. Researchers introduced the Dirichlet process (DP) as a prior over the number of driving behavior patterns that are probabilistically formulated by a hidden Markov model (HMM). Hamada, *et al.* [36] utilized beta process autoregressive HMM to segment driving behaviors into different states. Wang, *et*

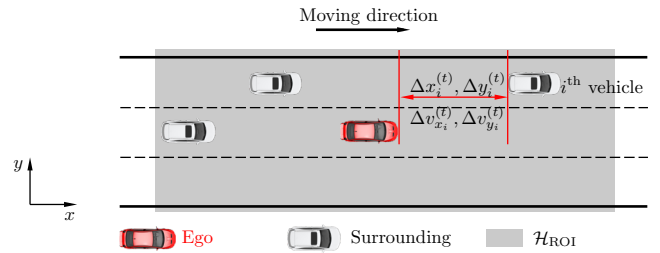


Fig. 2. Illustration of lane-change scenarios.

*al.* [22], [37] adopted a hierarchical DP-HMM to analyze the driving styles using multi-dimensional time-series driving data. Mahjoub, *et al.* [38] established a framework based on hierarchical DP to jointly model the driving behavior through forecasting the vehicle dynamical time-series. More theoretical basis of discrete Bayesian nonparametrics will be introduced in Section IV. In this paper, we combined the continuous and discrete Bayesian nonparametrics to learn interaction patterns during lane change from high-dimensional time series unsupervisedly.

## III. SPATIAL REPRESENTATION LEARNING OF MULTI-VEHICLE INTERACTIONS

Efficient representations of sequential interactions are critical to the performance of tasks [18] but challenging in the real-world as many time-varying factors exist in the dynamic scenarios such as the number of vehicles. Human brains can interact with their surroundings by actively forming a field of specific physiological/perceptual measures that reflect the behavioral relevance of a stimulus to actions [39]. Inspired by the above, the relevance between the driving environments and the driver's actions can reveal the human driver's interaction with other agents in the perception area. To construct this kind of representation, our previous work [40] introduced a Gaussian process regression model to estimate the influences of each vehicle's velocity at any location in the environment, termed as velocity fields. In [40], the authors assume that each vehicle has a symmetric impact on its nearby region, ignoring the intent of the surrounding vehicles, such as acceleration and deceleration. However, the brake action (deceleration) of a car would make a stronger impact on its behind area than its front area, and the left-turning maneuver would have a broader impact range on the left than on the right. In this section, we will first briefly revisit the model in our previous work [40] and then extend it to an acceleration-sensitive Gaussian velocity field by accounting for the impacts of driver intents.

### A. Gaussian Process and Velocity Fields

The surrounding vehicles in the environment (i.e., the pre-defined ROI,  $\mathcal{H}_{ROI}$ ) would have an impact on lane-change decisions and maneuvers of the ego vehicle. Different from existing works that aim to develop controllers and predict lane change behaviors [26]–[28], [41], [42], our focus is on capturing the interactions of the ego vehicle with other vehicles in the dynamic environments. We assume that the ego vehicle will not remain stationary to any surrounding obstacles

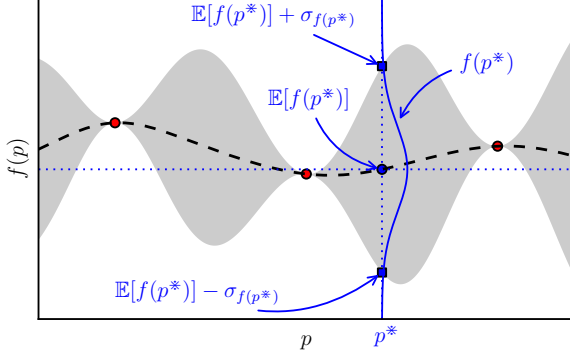


Fig. 3. Illustration of GPR in one dimension. Red dots are the observations  $\{p, f(p)\}$ .  $p$  and  $f(p)$  are the measure space of inputs and outputs, respectively. Black dash line represent the expectation of  $f(p)$ ,  $\mathbb{E}[f(p)]$ , for all  $p$ . The gray-shaded area represent the region  $\mathbb{E}[f(p)] \pm \sigma_{f(p)}$ .

during the entire lane-change process, and characterize the interactions using their relative velocity against positions.

Given  $N_t$  surrounding vehicles at time  $t$  ( $N_t$  is time-varying) in the environment space  $\mathcal{H}_{\text{ROI}}$  (see Fig. 2), the set of their location and relative velocity with respect to the ego vehicle is denoted by  $\{(x_n^{(t)}, y_n^{(t)})\}_{n=1}^{N_t}$  and  $\{(\Delta v_{x_n}^{(t)}, \Delta v_{y_n}^{(t)})\}_{n=1}^{N_t}$ , respectively. Our goal is to estimate the distribution of relative velocity over any location in  $\mathcal{H}_{\text{ROI}}$ . To simplify the model, we assume that the distributions in the directions of  $x$  and  $y$  are independent to each other. The estimation in either direction can be specified by Gaussian process regression (GPR). Thus, combining the distributions at two directions forms a Gaussian velocity field (GVF) over  $\mathcal{H}_{\text{ROI}}$ . More backgrounds refer to Chapter II in [43]. To help readers catch up the basic concept of the GVF, we first simply revisit the GPR for prediction with noise-free observations.

1) *GPR*: As the above discussion, the velocity distributions in the  $x$  and  $y$  directions at each location in  $\mathcal{H}_{\text{ROI}}$  are estimated independently. Hence, the GPR model in each direction is with inputs (i.e., location  $(x, y)$ ) in two dimensions and outputs (i.e.,  $\Delta v_x$  or  $\Delta v_y$ ) in one dimension. For simplification, we take a Gaussian process with one-dimensional output for illustration (see Fig. 3), defined as a probability distribution over function  $f(p) \in \mathbb{R}$  (Note that  $f(p)$  is a random variable for a specific  $p$ ) and  $p$  is the input. According to the definition of Gaussian process, any finite number of collections of random variables  $f(\cdot)$  still have a joint Gaussian distributions; for instance, any finite functional collections over  $p$  and  $p'$  have a Gaussian distribution

$$f(p) \sim \mathcal{N}(\mu(p), k(p, p')) \quad (1)$$

with the mean function  $\mu(p)$  and the covariance function  $k(p, p')$ <sup>1</sup>, computed by

$$\mu(p) = \mathbb{E}[f(p)] \quad (2a)$$

$$k(p, p') = \mathbb{E}[(f(p) - \mu(p))(f(p') - \mu(p'))] \quad (2b)$$

<sup>1</sup>The covariance function  $k(p, p')$  can be treated as the simplified form of  $\text{cov}(f(p), f(p'))$  – the covariance of functional random variables  $f(p)$  and  $f(p')$ .

Note that when  $p = p'$ ,  $k(p, p') = \sigma_{f(p)}$  is the standard variance of the functional variable  $f(p)$ . Fig. 3 illustrates an example of the GPR in one dimension.

Assuming that we have the observation set  $\{p_n, f(p_n)\}_{n=1}^N$ , our aim is to estimate the distribution of  $\{f(p_m^*)\}$  over any finite collections of possible inputs  $\{p_m^*\}_{m=1}^M$ . For simplification, we denote  $\mathbf{p} = [p_1, \dots, p_N]$ ,  $\mathbf{f} = [f(p_1), \dots, f(p_N)]$ ,  $\mathbf{p}^* = [p_1^*, \dots, p_M^*]$ , and  $\mathbf{f}^* = [f(p_1^*), \dots, f(p_M^*)]$ . According to the attribute of Gaussian process, both of  $\mathbf{f}$  and  $\mathbf{f}^*$  are the instantiation of the finite collections of random variables and thus have Gaussian distributions. The prior knowledge about the mean of  $\mathbf{f}$  is unavailable, therefore, we set the prior distributions of  $\mathbf{f}$  and  $\mathbf{f}^*$  with zero-mean value as

$$\mathbf{f} \sim \mathcal{N}(\mathbf{0}, \mathbf{K}(\mathbf{p}, \mathbf{p})) \quad (3a)$$

$$\mathbf{f}^* \sim \mathcal{N}(\mathbf{0}, \mathbf{K}(\mathbf{p}^*, \mathbf{p}^*)) \quad (3b)$$

where  $\mathbf{K}$  is the covariance matrix with elements  $k_{ij} = k(p_i, p_j)$ . Given noise-free training data  $\{p_i, f(p_i)\}$ , the joint distribution of the training outputs  $\mathbf{f}$  and the test outputs  $\mathbf{f}^*$  still has a zero-mean Gaussian distribution with

$$\begin{bmatrix} \mathbf{f} \\ \mathbf{f}^* \end{bmatrix} \sim \mathcal{N}\left(\mathbf{0}, \begin{bmatrix} \mathbf{K}(\mathbf{p}, \mathbf{p}) & \mathbf{K}(\mathbf{p}, \mathbf{p}^*) \\ \mathbf{K}(\mathbf{p}^*, \mathbf{p}) & \mathbf{K}(\mathbf{p}^*, \mathbf{p}^*) \end{bmatrix}\right) \quad (4)$$

with  $\mathbf{K}(\mathbf{p}, \mathbf{p}) \in \mathbb{R}^{N \times N}$ ,  $\mathbf{K}(\mathbf{p}, \mathbf{p}^*) \in \mathbb{R}^{N \times M}$ ,  $\mathbf{K}(\mathbf{p}^*, \mathbf{p}) \in \mathbb{R}^{M \times N}$ , and  $\mathbf{K}(\mathbf{p}^*, \mathbf{p}^*) \in \mathbb{R}^{M \times M}$ .

Here, we aim to sample from the posterior distribution which contains the information from the training data, rather than draw random functions directly from the prior. According to the multivariate conditional Gaussian distribution with (4), the mean and the covariance of the distribution of test outputs conditioning on the training outputs are given by

$$\mathbf{f}^* | \mathbf{p}^*, \mathbf{p}, \mathbf{f} \sim \mathcal{N}(\boldsymbol{\mu}_{\mathbf{f}^*}, \boldsymbol{\Sigma}_{\mathbf{f}^*}) \quad (5)$$

with

$$\boldsymbol{\mu}_{\mathbf{f}^*} = \mathbf{K}(\mathbf{p}^*, \mathbf{p})\mathbf{K}(\mathbf{p}, \mathbf{p})^{-1}\mathbf{f} \quad (6a)$$

$$\boldsymbol{\Sigma}_{\mathbf{f}^*} = \mathbf{K}(\mathbf{p}^*, \mathbf{p}^*) - \mathbf{K}(\mathbf{p}^*, \mathbf{p})\mathbf{K}(\mathbf{p}, \mathbf{p})^{-1}\mathbf{K}(\mathbf{p}, \mathbf{p}^*) \quad (6b)$$

Therefore, given any input  $p$ , the distribution of functional random variable  $f(p)$  of any other possible input  $p^*$  over the input space can be computed directly.

2) *Gaussian Velocity Fields (GVF)*: To describe the probability of multi-vehicle interactions at any location in a predefined ROI, we introduce the GPR to compute their estimates. The interaction at any location is specified by their relative velocities between the ego vehicle and the surrounding vehicles against their relative positions. For computational efficiency, the estimated relative velocity in the  $x$  and  $y$  directions at a single location is independent of each other. In what follows, we compute the interaction in the  $x$  direction, which is also applicable for estimation in the  $y$  direction.

Given the training data  $\{(\Delta v_x(p_i), \Delta v_y(p_i))\}_{i=1}^{N_t}$  at associated locations  $\mathbf{p} = \{p_i\} = \{(x_i, y_i)\}_{i=1}^{N_t} \in \mathcal{H}_{\text{ROI}}$  at time  $t$ , we assume all the functional random variables over  $\mathcal{H}_{\text{ROI}}$  are Gaussian process. Thus, we can compute the distribution of  $\Delta v_x$  at a finite number of collections of any possible locations  $\mathbf{p}^*$  by

$$\Delta v_x(\mathbf{p}^*) \sim \mathcal{N}(\boldsymbol{\mu}_x(\mathbf{p}^*), \boldsymbol{\Sigma}_x(\mathbf{p}^*)), \forall \mathbf{p}^* \in \mathcal{H}_{\text{ROI}} \quad (7)$$



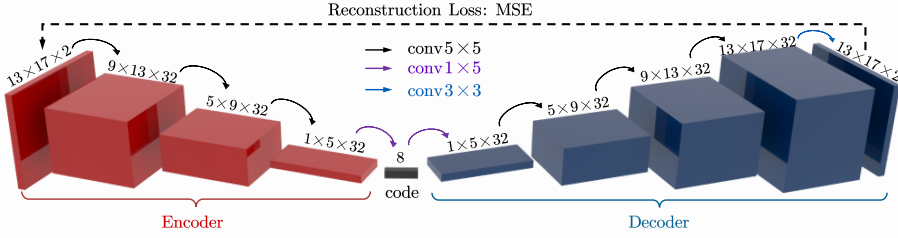


Fig. 4. Architecture of the convolutional autoencoder and its settings.

where  $\mu_x(\mathbf{p}^*)$  is the mean value of  $\Delta v_x(\mathbf{p}^*)$  and  $\Sigma_x(\mathbf{p}^*)$  is the covariance. Different from (2b) in one dimension, each element of  $\Sigma_x(\mathbf{p}^*)$  is specified by a multivariate kernel  $k(p_i, p_j)$  with  $p_i, p_j \in \mathbf{p}^*$ , and  $k$  is defined as the standard squared exponential function

$$k(p_i, p_j) = A \cdot \exp\left(-\frac{(x_i - x_j)^2}{2\sigma_x^2} - \frac{(y_i - y_j)^2}{2\sigma_y^2}\right) \quad (8)$$

where  $A$  is an amplitude constant,  $\sigma_x$  and  $\sigma_y$  are length-scale constant controlling how the correlations are decay with respect to distance. A larger value of  $\sigma_x$  (or  $\sigma_y$ ) indicates slow decay and thus farther points will have near-zero covariance or correlations. The selection of the standard squared exponential kernel is that the nearby relative velocity samples are more correlated than the one farther away in the field of  $\mathcal{H}_{ROI}$ .

Therefore, according to (6a), given the sets of relative velocity  $\Delta \mathbf{V}_x = \{\Delta v_x(p_i)\}_{i=1}^{N_t}$  at locations  $\mathbf{p}$  of all surrounding vehicles as the training data, the posterior distribution of the predicted relative velocities  $\Delta v_x(\mathbf{p}^*)$  at any location  $\mathbf{p}^*$  in the ROI can be efficiently computed by

$$\mu_x(\mathbf{p}^*) = \mathbf{K}(\mathbf{p}^*, \mathbf{p})\mathbf{K}(\mathbf{p}, \mathbf{p})\Delta \mathbf{V}_x, \quad \mathbf{p}^* \in \mathcal{H}_{ROI} \quad (9)$$

Similarly, we can obtain the distribution of relative velocity at a finite collection of any location  $\mathbf{p}^*$ , denoted as  $\mu_y(\mathbf{p}^*)$ .

After computing the expectation of the relative velocity in the  $x$  and  $y$  directions independently, we can estimate the value and direction of the relative velocity at any location in the ROI.

### B. Acceleration-Sensitive GVF (AS-GVF)

The above section describes the representation of multi-vehicle interactions based on the GVF specified by the relative velocity of agents in the surrounding area. Each vehicle impact on their surroundings symmetrically according to (8), which leads to the deviation from the real traffic situation as humans are also active to stimulus (e.g., acceleration) other than proximity [39]. For example, a nearby moving vehicle would draw a non-symmetric stimulus on its surrounding space for the human drivers due to maneuvers such as deceleration and acceleration [44]. To make the distance-based GVF discussed above capable of capturing the inertia of vehicle motion, we revise the symmetric and isotropic kernel of (8) by integrating the acceleration of surrounding vehicles.

The modified velocity field is expected to reflect driving intent and instant stimulus of each surrounding vehicle in the environment. To this end, we consider the influence of acceleration/deceleration to depict the motion tendencies of

each surrounding vehicle. We reconstructed (9) by integrating the acceleration/deceleration into  $\mathbf{K}$  through a skewed matrix  $\mathbf{K}'$ , thus obtaining

$$\mu'_x(\mathbf{p}^*) = \underbrace{\mathbf{K}'(\mathbf{p}^*, \mathbf{p}, \mathbf{a}_x, \mathbf{a}_y) \circ \mathbf{K}(\mathbf{p}^*, \mathbf{p})}_{\text{Hadamard product}} \mathbf{K}(\mathbf{p}, \mathbf{p})\Delta \mathbf{V}_x \quad (10)$$

where  $\circ$  represents the Hadamard product,  $\mathbf{a}_x$  and  $\mathbf{a}_y$  are the set of accelerations in the  $x$  and  $y$  directions, respectively. The skewed matrix is

$$\mathbf{K}' = \begin{bmatrix} k'_{1,1} & \cdots & k'_{1,N_t} \\ \vdots & \ddots & \vdots \\ k'_{M,1} & \cdots & k'_{M,N_t} \end{bmatrix}_{M \times N_t}$$

with  $k'_{ij} = k'(p_i, p_j, \mathbf{a}_j)$ ,  $\mathbf{a}_j = [a_{j,x}, a_{j,y}]$ ,  $j \in \{1, \dots, N_t\}$ , and  $i \in \{1, \dots, M\}$ , where  $N_t$  is the number of vehicles in the environment at time  $t$ , and  $M$  is the number of testing locations in the  $x$  or  $y$  directional space over  $\mathcal{H}_{ROI}$ . Therefore, the skew matrix is in  $\mathbb{R}^{M \times N_t}$ . In order to make  $k'_{ij}$  practically feasible, two constraints of acceleration should be satisfied

- A vehicle heading straight with small acceleration would have an almost symmetric influence over the environment. As the acceleration approaches to zero, the value of AS-GVF would converge to GVF.
- An aggressive acceleration/deceleration would lead to a high (low) field density in the (opposite) direction of the acceleration.

Therefore, we define  $k'_{ij}$  as a function of the relative position and acceleration and with a high value in the accelerating direction. Here,  $k'$  is designed by multiplying two logistic functions in the direction of  $a_x$  and  $a_y$  as

$$k'(p_i, p_j, \mathbf{a}_j) = \prod_{\ell=x,y} \frac{\xi_\ell}{1 + e^{-\lambda_\ell a_{j,\ell}(\ell_i - \ell_j)}} \quad (11)$$

where  $\xi_\ell$  is the normalization factor and  $\lambda_\ell$  is the skewing factor.

### C. Dimension Reduction of AS-GVF

The developed AS-GVF captures the multi-vehicle interactions using the estimated relative velocity at each location in the environment, which can be formed as a tensor. However, a high-dimensional tensor makes it computationally infeasible to implement Bayesian inference with sampling algorithms. Therefore, reducing the high-dimensional tensor into a low dimension is a prerequisite for efficient recognition of interaction patterns.

In this paper, we implemented an unsupervised technique – convolutional autoencoder (CAE) to generate latent codes to represent AS-GVF at each time. A typical autoencoder is composed of an encoder  $h = g_1(s)$  and a decoder  $r = g_2(h)$ . It reconstructs its inputs  $s$  and sets the target values of output  $\hat{s} = g_2(g_1(s))$  to be equal to  $s$ , where  $g_1(\cdot)$  and  $g_2(\cdot)$  are the activation functions [45]. The tensor of AS-GVF characterizes the spatial interactions of vehicles in the environment, thus a convolutional operation over the velocity field can take satisfied performance of feature extraction. In our case, the CAE is treated as a deep autoencoder with fully convolutional layers, as shown in Fig. 4.

#### IV. SPATIOTEMPORAL INTERACTION PATTERNS LEARNING

The AS-GVF as above described delivers the feature representatives of multi-vehicle interactions at each frame. Our goal is to cluster the sequential interactions into groups according to the similarity. However, it is infeasible to manually set the number of interaction patterns due to the growth of data. This section will describe a discrete Bayesian nonparametric approach to segment the behavioral sequences into fundamental pieces, called primitives [40], [46], while clustering them into groups. We first revisit the basic concept of primitives and then introduce the related Bayesian nonparametric methods to learn them.

##### A. Primitives and Interaction Patterns

Human skills consist of primitive information processing elements and several of these primitive elements are necessary for even a single step in a task [47]. Besides, segmenting complex interactive behavioral sequences into recognizable small elements gives an insight into driving behavior recognition and prediction [36], [48]. Supported by these conclusions, the multi-vehicle sequential interactions during lane change can be segmented into a bunch of cascading fundamental blocks (i.e., primitives). More specifically, the primitives in this paper are referred to as the segments of the sequential interaction behavior during lane change over time. Therefore, each type of primitives represents a kind of essential lane-change interaction pattern, and a complex lane-change scenario consists of several types of traffic primitives or interaction patterns.

##### B. Bayesian Nonparametric Models

The number of interaction patterns during lane change, intuitively, should increase as more new scenarios being explored. This kind of functionality can be achieved with nonparametric models whose parameters will theoretically increase with more data get observed. In this paper, we implement a nonparametric model in a Bayesian framework with an infinite-dimensional parameter space. Besides, we assume that during the lane-change procedure, the sequential interactions has the Markov property, which makes it tractable to employ a hidden Markov model (HMM) to formulate the dynamic transition of these interaction patterns. Another expected capability of Bayesian nonparametric models is grouping these patterns while taking segmentation, which could be carried out by introducing a

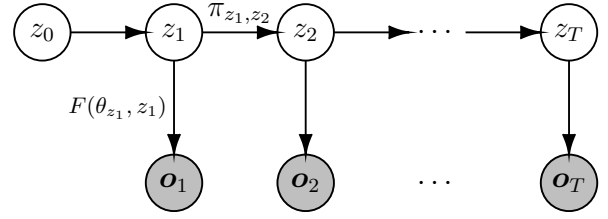


Fig. 5. The graphical illustration of hidden Markov models.

hierarchical Dirichlet process (HDP) over HMM, called as HDP-HMM [49]. In what follows, we will revisit the relevant theoretical preliminaries.

1) *Hidden Markov Model*: As the lane-change interaction behavior is treated as a certain cascade of sequential interaction patterns, the dynamic process among these patterns can be modeled as a probabilistic inferential process. Specifically, we model the dynamics of interaction patterns over the time horizon based on the structure of HMM, which includes two parts (see Fig. 5): discrete latent interaction patterns (denoted by non-shaded nodes  $z_t$ ) and observed interaction representations (denoted by shaded nodes  $o_t$ ). Our learning task aims to infer the latent pattern from the observed interaction representations. In the HMM, each observed interaction representation  $o_t$  at time  $t$  would be assigned an interaction pattern  $z_t \in \mathcal{Z}$ , where  $\mathcal{Z}$  is the set of all types of interaction patterns. For convenient formulation, we specify each type of pattern in  $\mathcal{Z}$  using an integer number, i.e.,  $z_t$  is equal to any single element in  $\{1, 2, \dots, |\mathcal{Z}|\}$ , where  $|\mathcal{Z}|$  is the size of the set  $\mathcal{Z}$ . The probability that the pattern at time  $t$  transits to the pattern at time  $t + 1$  is denoted by  $\pi_{z_t, z_{t+1}}$ , which is shortened as  $\pi_{i,j}$  when  $z_t = i$  and  $z_{t+1} = j$  with  $i, j \in \mathcal{Z}$ . Thus,  $\pi = \{\pi_{i,j}\}_{i,j=1}^{|\mathcal{Z}|}$  is the probabilistic transition matrix, and  $\pi_i$  represents the probability of transiting from pattern  $i$  to any other patterns. According to the above definition, given current latent pattern  $z_t$  and the emission parameter  $\theta_{z_t}$ , the observed representation  $o_t$  is drawn from a function  $F(o_t | \theta_{z_t}, z_t)$  parameterized by  $\theta_{z_t}$ . Then, the general form of HMM can be written as

$$z_t | z_{t-1} \sim \pi_{z_{t-1}} \quad (12a)$$

$$o_t | z_t \sim F(\theta_{z_t}, z_t) \quad (12b)$$

where  $\pi_{z_{t-1}}$  represents the distribution of  $z_t$  conditional on the one-step-back latent pattern  $z_{t-1}$ . The classical treatments of HMM require to specify the size of  $\mathcal{Z}$ ; however, in our problem,  $|\mathcal{Z}|$  is unknown a priori – we do not exactly know how many interaction patterns exist in a bunch of sequential lane-change behaviors. To solve this problem, we introduce a discrete prior probability distribution in infinite-dimensional space based on Dirichlet Processes (DP).

2) *DP and Hierarchical DP*: To construct a valid probability measure  $\pi_{z_{t-1}}$  (in Equation (12a)) that can describe the transition probability while automatically increasing the number of interaction patterns and synchronously assigning new pattern parameters  $\theta_{z_t}$  (in Equation (12b)) with new data get observed incrementally, we introduce the Dirichlet process

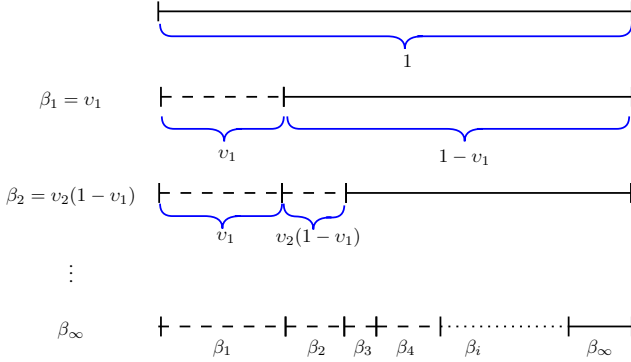


Fig. 6. Illustration of the stick-breaking model to construct  $\beta$  for  $\text{GEM}(\gamma)$ . The probabilities of  $\beta_k$  are given by a procedure resembling the breaking of a unit-length stick  $\beta_k = v_k \prod_{i=1}^{k-1} (1 - v_i)$  with  $v_k$  independently drawn from a Beta distribution,  $\text{Beta}(1, \gamma)$ .

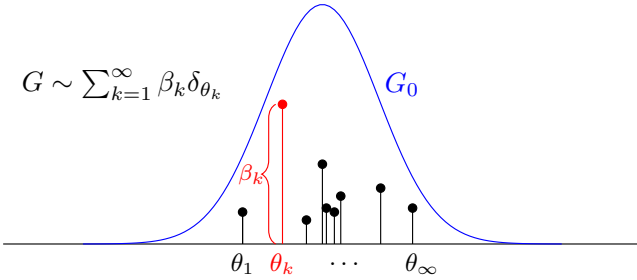


Fig. 7. Illustration of DP construction with a continuous base measure  $G_0$ . The sum of the height of all the vertical lines is equal to one when  $k \rightarrow \infty$ .

(DP) over an infinite measure space as the basis. The DP can be constructed by two independent valid probability measures:

$$G \sim \sum_{k=1}^{\infty} \beta_k \delta_{\theta_k} \quad (13)$$

where  $[\beta_1, \beta_2, \dots]$  are drawn from the  $\text{GEM}(\gamma)$  distribution<sup>2</sup> with  $\sum_{i=1}^{\infty} \beta_i = 1$ , i.e.,  $\beta \sim \text{GEM}(\gamma)$  (see Fig. 6), and  $\theta_k$  is drawn from a base measure  $G_0$ . The  $\delta_{\theta_k}$  is the Dirac delta measure and denotes a point mass at  $\theta_k$ . Note that the base measure  $G_0$  can be continuous or discrete, but  $G$  is a discrete probability measure due to the Dirac delta measure. Moreover, both  $\beta_k$  and  $\theta_k$  are random, thus indicating that  $G$  becomes a random probability measure and can be rewritten in the form of DP,  $G \sim \text{DP}(\gamma, G_0)$ . The above discussion implies that  $\gamma$ , called concentration parameter, governs how close the random probability measure  $G$  is to the base measure  $G_0$ .

A group of discrete distributions  $G$  drawn from  $\text{DP}(\gamma, G_0)$  directly with a specific base measure  $G_0$  would not share atoms across different  $G$  as the  $G_0$  is continuous – the probability of drawing two points with the same value from a continuous space is zero. In order to make the atoms  $(\{\theta_k\})$  among  $G$  are shareable, we add another DP layer to discretize the continuous base measure  $G_0$ , thus reshaping a hierarchical Dirichlet process (HDP) [50].

<sup>2</sup>The Griffiths-Engen-McCloskey (GEM) distribution is a special case of DP, which can be reconstructed via the stick-breaking model.

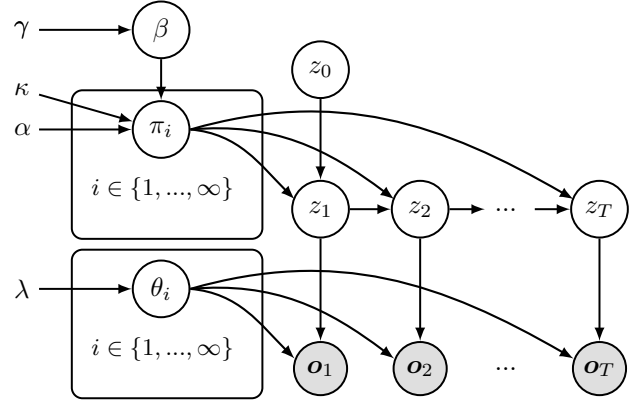


Fig. 8. The graphical model of the sticky HDP-HMM. Gray-filled circles represent the learned representations, the white circles are the random variables, and the box denotes a set of infinite collections of random variables.

3) *Sticky HDP-HMM*: In HDP, we expect that the transition of interaction patterns between two adjacent data frames is adjustable and has a low frequency. Therefore, an extra sticky parameter  $\kappa > 0$  is added to bias the process toward self-transition in the HDP, called the sticky HDP. Thus, placing a sticky HDP prior over infinite transition matrices of HMM, we obtain a sticky HDP-HMM( $\kappa, \alpha, H$ ) [49] (as shown in Fig. 8), formulated as

$$\beta | \gamma \sim \text{GEM}(\gamma) \quad (14a)$$

$$\pi_i | \alpha, \beta, \kappa \sim \text{DP}\left(\alpha + \kappa, \frac{\alpha \beta + \kappa \delta_i}{\alpha + \kappa}\right), i = 1, 2, \dots \quad (14b)$$

$$z_t | z_{t-1} \sim \pi_{z_{t-1}}, t = 1, 2, \dots, T \quad (14c)$$

$$o_t | z_t, \theta_{z_t} \sim F(\theta_{z_t}, z_t), t = 1, 2, \dots, T \quad (14d)$$

$$\theta_i | H \sim H, i = 1, 2, \dots \quad (14e)$$

After built the generative model above, we need to infer the model parameters based on sequential representatives of multi-vehicle interactions. In this paper, we implemented a weak-limit Gibbs sampling algorithm for the sticky HDP-HMM [51]. The observation function  $F(\theta_{z_t})$  is treated as a Gaussian distribution specified by  $\theta_{z_t} = [\mu_{z_t}, \Sigma_{z_t}]$ , we take  $\mu_{z_t} = 0$  according to [36] and the self-transition parameter  $\kappa = 0.25$ . The hyperparameters  $\alpha$  and  $\gamma$  are drawn from a gamma prior in order to make the posterior distribution computationally tractable, and the hyperparameters for  $\theta$  are determined by an Inverse-Wishart (IW) distribution [37].

## V. DATA PROCESSING AND EXPERIMENTAL RESULT ANALYSIS

### A. Data Preprocessing

In this paper, we trained and validated our proposed framework using the lane-change data from the released dataset – the Highway Drone (highD) Dataset [52]. The highD dataset has 60 video recordings, logged with the sampling frequency of 25 Hz, consisting of two different environment settings (see Fig. 9): four-lane divided and six-lane divided. We selected one record for each environment setting – Recording03 for the four-lane divided highway and Recording07 for the six-lane divided highway, as shown in Table I. To save the use of

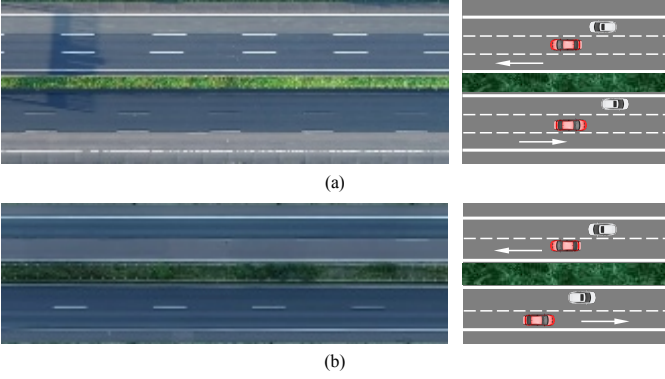


Fig. 9. Illustrations of (a) the six-lane divided highway and (b) the four-lane divided highway in the highD dataset.

TABLE I  
METADATA FOR THE HIGHD DATASET.

	Recording03	Recording07	Total
Total vehicles	914	855	1769
Lane-change vehicles	119	130	249
Total frames	303488	257031	560519
Lane-change frames*	35333	37270	72603

\* All the frames of lane-change vehicles.

memory, we downsampled the raw sequential frames to 5 Hz, thus obtaining 14563 frames of all lane-change vehicles.

Furthermore, the  $y$ -axis in the highD dataset is heading down and different from what we defined in Fig. 2, we transformed the original coordinate system by rotating the  $y$ -axis in 180 deg clock-wisely. Meanwhile, we also rotated the coordinates of the heading-left vehicles in 180 deg clock-wisely. After this pre-processing, the move directions of all vehicles are unified (i.e., heading right), and the coordinates in some results could be found with negative values.

### B. AS-GVF Feature Representation

In the AS-GVF, we define  $\mathcal{H}_{\text{ROI}}$  as a rectangle area symmetrically centered on the ego vehicle and specified by three distances against the center of the ego vehicle (see Fig. 10): the front distance,  $d_{\text{front}}$ , the behind distance,  $d_{\text{behind}}$ , and the left/right distance  $d_{\text{side}}$ . The lane width is around 4 m in the environment, therefore we set the left/right distance as  $d_{\text{side}} = 6$  m and can covers the driving lane exactly, including the left and right lanes. For the longitudinal observation distances, we select a medium distance gap according to [53] and set  $d_{\text{front}} = d_{\text{behind}} = 40$  m. Theoretically, the range of the defined ROI could be infinite, seeing that the length and width of the ROI can be meshed into as many grids as expected. Considering the computational feasibility, the AS-GVF is constructed on the crossing points in the ROI by meshing the width and length using intervals of 1 m and 5 m, respectively. Thus, the size of testing locations in  $\mathcal{H}_{\text{ROI}}$  for our AS-GVF along the  $x$  and  $y$  directions are 17 and 13, respectively. In this way, a tensor with a size of  $13 \times 17 \times 2$  can describe the AS-GVF of each frame, where 2 represents the velocity components in the  $x$  and  $y$  directions. In the AS-GVF

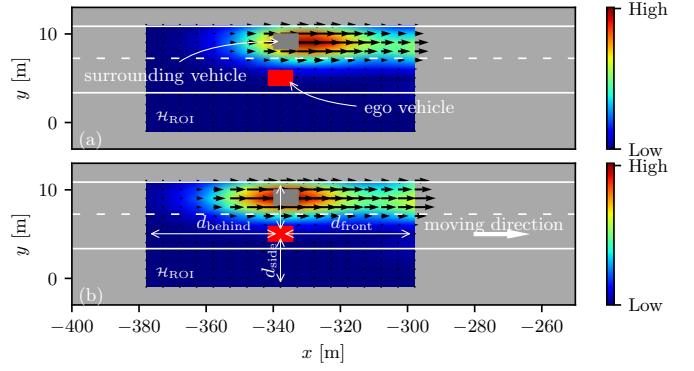


Fig. 10. Comparison of (a) our AS-GVF considering acceleration sensitivity with (b) the conventional GVF.

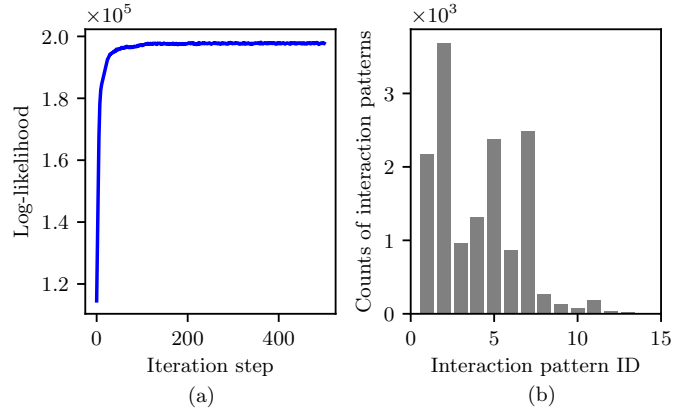


Fig. 11. (a) The log-likelihood of training data with respect to the iterations and (b) the histogram of the number of interaction patterns during lane change.

model, we set  $A = 1$ ,  $\sigma_x = 15$  m,  $\sigma_y = 1.5$  m,  $\lambda_x = 0.6$ , and  $\lambda_y = 0.9$ .

Fig. 10 compares our AS-GVF with the conventional GVF regarding the capability of representing multi-vehicle interactions, in which the ego vehicle is heading to the right while the surrounding vehicle is accelerating and trying to overtake. Black arrows represent the direction and size of the estimated relative velocity  $(\Delta v_x, \Delta v_y)$  at any location in  $\mathcal{H}_{\text{ROI}}$  according to the observed relative speed of these two vehicles and their states. Comparison verifies that the conventional GVF can only capture the symmetric influence of the surrounding vehicle on its surroundings but ignore the influence of acceleration of the vehicle, as shown by the symmetric heatmap in Fig. 10(b). However, our developed AS-GVF can account for the influence of acceleration on its nearby region of the surrounding vehicle, as shown in Fig. 10(a). The surrounding vehicle has a higher density (i.e., a stronger influence) at its front area than its behind due to the accelerating maneuvers. In summary, our developed AS-GVF is flexible to adapt to the driving intent via the incorporation of acceleration/deceleration.

### C. Convolutional Autoencoder

Fig. 4 details the CAE architecture we implemented, which is constructed in the form of an asymmetric structure as we



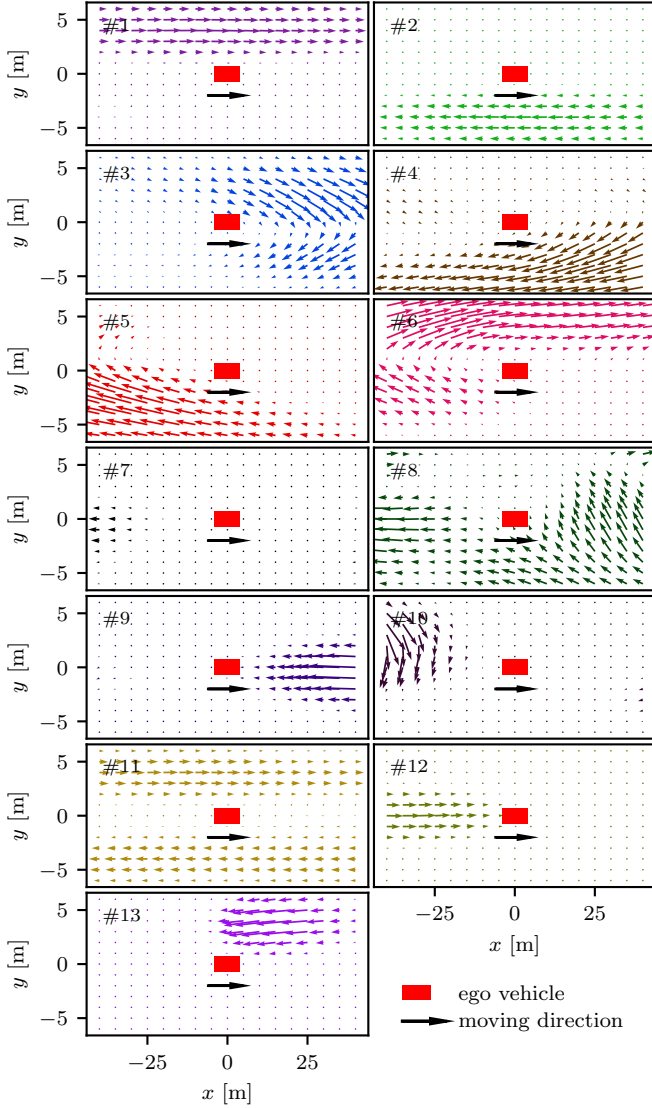


Fig. 12. The representative fields of the learned 13 patterns. The red-shaded rectangles represent the ego vehicle which is moving toward the right direction.

added an extra transpose convolutional layer before the output layer. We used the Nesterov-accelerated Adaptive Moment Estimation (Nadam) algorithm [54] to optimize our model with a mini-batch size of 1024 on NVIDIA TESLA P40. All of the 14563 frames are set as training data. We used the mean squared error (MSE) as the reconstruction loss function, which is reduced to as low as  $8.77 \times 10^{-5}$  after  $2 \times 10^4$  iterations.

In order to build a representative feature that can both capture the interaction of the ego vehicle with their surroundings and their driving behavior at each frame, we use the combination (denoted as  $\mathbf{o}$ ) of the ego vehicle state  $[v_x, v_y, a_x, a_y]^T \in \mathbb{R}^{4 \times 1}$  and the extracted latent codes  $h \in \mathbb{R}^{8 \times 1}$  via CAE. Thus, the combination over all frames forms a sequential representation  $O = \{\mathbf{o}_1, \dots, \mathbf{o}_T\}$  with a size of  $12 \times T$ , where  $\mathbf{o}_t \in \mathbb{R}^{12 \times 1}$  is the synthesized feature of interactions at time  $t$ , and  $T$  is the total number of after-processing frames,  $T = 14563$ .

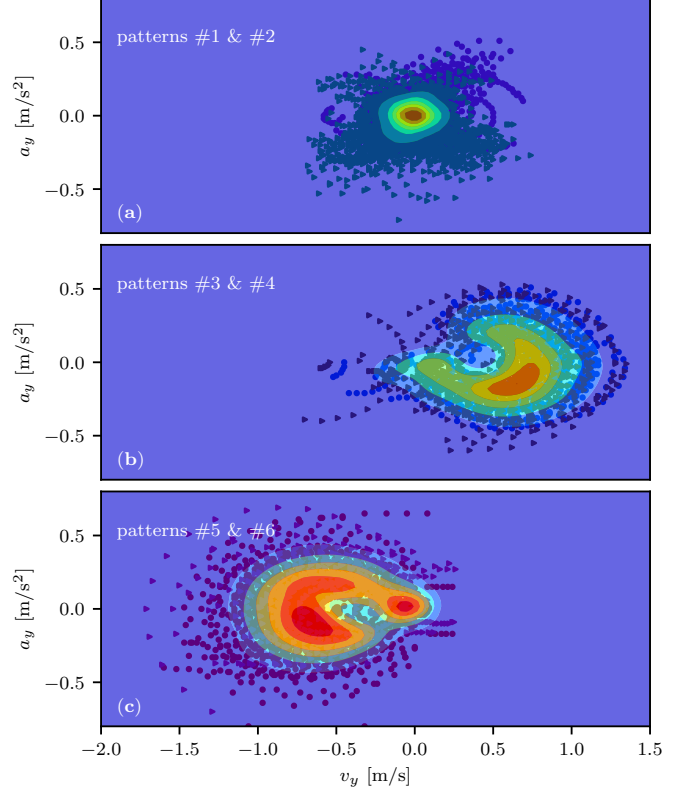


Fig. 13. The distribution of lateral operation states for six typical patterns #1 – #6 in the  $v_y - a_y$  coordinates.

#### D. Interaction Pattern Learning and Spatial Analysis

To segment the sequential lane-change interaction scenarios, the above extracted sequential features  $O$  are treated as the training data, and passed through the sticky HDP-HMM [51] by maximizing the training iteration step as 500. Fig. 11(a) shows the log-likelihood of the data with parameter updates along the training iterations. It indicates that the training procedure is convergent. Fig. 11(b) shows the totally 13 types of interaction patterns during lane change, from which we know that during lane-change scenarios, human drivers interact with their surrounding vehicles by following patterns #1 – #7 more frequently than following patterns #8 – #13.

Fig. 12 lists all types of interaction patterns with velocity fields distinguished by colors, which enables the interpreting of these patterns on how they characterize the interactions of the ego vehicle with their surrounding vehicles. Each subplot is computed by averaging all of the velocity fields with the same pattern label. The colored arrows represent the estimated relative velocity at any location in  $\mathcal{H}_{ROI}$ , and a long arrow indicates a high relative speed with respect to the ego vehicle at that location. In what follows, we will semantically interpret each interaction pattern.

Pattern #1 (Pattern #2) describes that a surrounding vehicle is moving faster (slower) in the adjacent left-hand (right-hand) lane, thus causing a relative velocity pointing in the head-forward (backward) direction. The opposite sides of both patterns – the adjacent right-hand lane in pattern #1 and

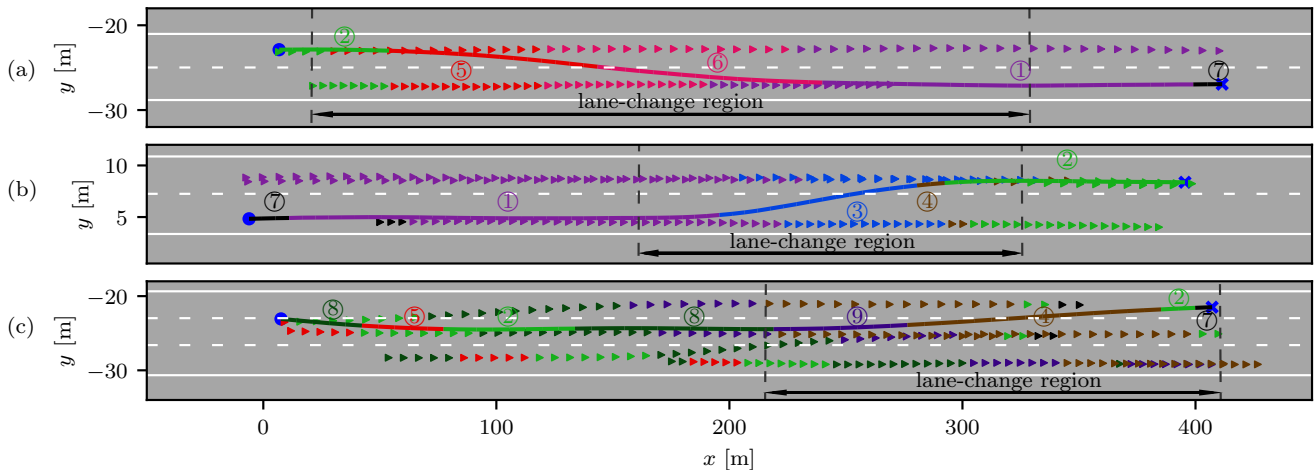


Fig. 14. Three examples of illustrating the dynamic process over interaction patterns during lane change in different road contextual settings: (a), (b) four-lane divided highway and (c) six-lane divided highway. While solid and dashed line – Lane marker; Circled number – Pattern ID; Colored solid line – Trajectory of the ego vehicle; Filled triangle (►) – Trajectory of surrounding vehicles; Blue dot (●) – Start position of the ego vehicle; and Blue cross (×) – End position of the ego vehicle.

the adjacent left-hand lane in pattern #2 – possess near-zero arrows, indicating that there are no vehicles on associated lanes, or that some vehicles are on the associated lanes but with a near-zero relative velocity to the ego vehicle. In these two interaction patterns, the human driver keeps moving on the current driving lane straightly, therefore, it leads a imperceptible tendency of lateral moving. Correspondingly, Fig.13(a) shows the distribution of the lateral moving states  $[v_y, a_y]$  of the ego vehicle, and illustrates that all states are almost falling around (0,0) – both the lateral speed and acceleration are near-zero. Further, these two interaction patterns typically occur in the preparing stage of lane change, as shown in Fig. 14. One interesting finding is that pattern #11 is likely the combination of patterns #1 and #2. It only occurs on the six-lane divided highway (see Fig. 9(a)) as it describes the interaction scenario in which the ego vehicle is moving faster than the vehicles on its adjacent right-hand lane while slower than the vehicles on its adjacent left-hand lane.

Pattern #3 represents the scenario that the ego vehicle starts accelerating and operating the vehicle to approach to the adjacent left-hand lane – giving up following the slow leading vehicle on the current lane – as the head of arrows at the left front area of the ego vehicle is pointing in the right front direction. Fig. 14(b) shows an associated real-world case for pattern #3. While pattern #4 represents that the ego vehicle is changing lanes to the left, as shown in Fig. 14(b) and (c). Different from pattern #3 in which the right side area of the ego vehicle possesses near-zero arrows, pattern #4 possesses near-zero arrows at the left side area of the ego vehicle, indicating that no vehicles exist on the left-hand target lane. Correspondingly, Fig. 13(b) shows the states of the ego vehicle regarding patterns #3 and #4, which implies that most left lane-change cases are specified by a positive  $v_y$  and a negative  $a_y$ .

Pattern #5 describes that the ego vehicle is moving faster and passing a slower vehicle on its right side during lane

change, while no vehicles exist in its left front area. In pattern #6, the ego vehicle is almost in the target lane and overtaking a slow vehicle; moreover, it represents the behavior of giving ways to other faster vehicles on the left lane, as shown in Fig. 14(a). The distribution of the ego vehicle's states corresponding to patterns #5 and #6 is given in Fig. 13(c), which implies that the ego vehicle slightly moves in the right direction during lane change, accompanying with a negative lateral speed  $v_y$ .

Pattern #7 describes a special interaction case, in which there is no obvious relative movement in the ROI because the length of arrows is close to zero. This interaction pattern typically occurs at the very beginning or ending of the lane-change procedure, as shown in Fig. 14. This explains why pattern #7 has a large proportion in all interaction patterns, as displayed in Fig. 11(b).

Pattern #8 represents two cases: 1) the ego vehicle is cutting in to the adjacent right-hand lane and 2) the right leading vehicle is cutting in to the front area of the ego vehicle. Thus, the arrow behind the ego vehicle in the ROI is pointing in the opposite moving direction – that is, the behind following vehicle decelerates to guarantee an appropriate safety gap – while the arrows in the front right side of the ego vehicle are pointing in the left behind direction. Correspondingly, pattern #10 describes the opposite view of the right leading vehicle in pattern #8. These cases typically occurs in the extreme cluttered scenarios with a mess of surrounding vehicles, as shown in Fig. 14(c).

Both of patterns #9 and #12 represent that the ego vehicle and the surrounding vehicle are approaching each other in the same lane. However, the ego vehicle in pattern #9 is getting closer to the rear side of the ahead vehicle while the behind following vehicle in pattern #12 is chasing the ego vehicle in the same direction. Pattern #13 describes that the ego vehicle on the current lane drives faster than the surrounding vehicle on its adjacent left-hand lane, which is also a typical scenario in real-world.

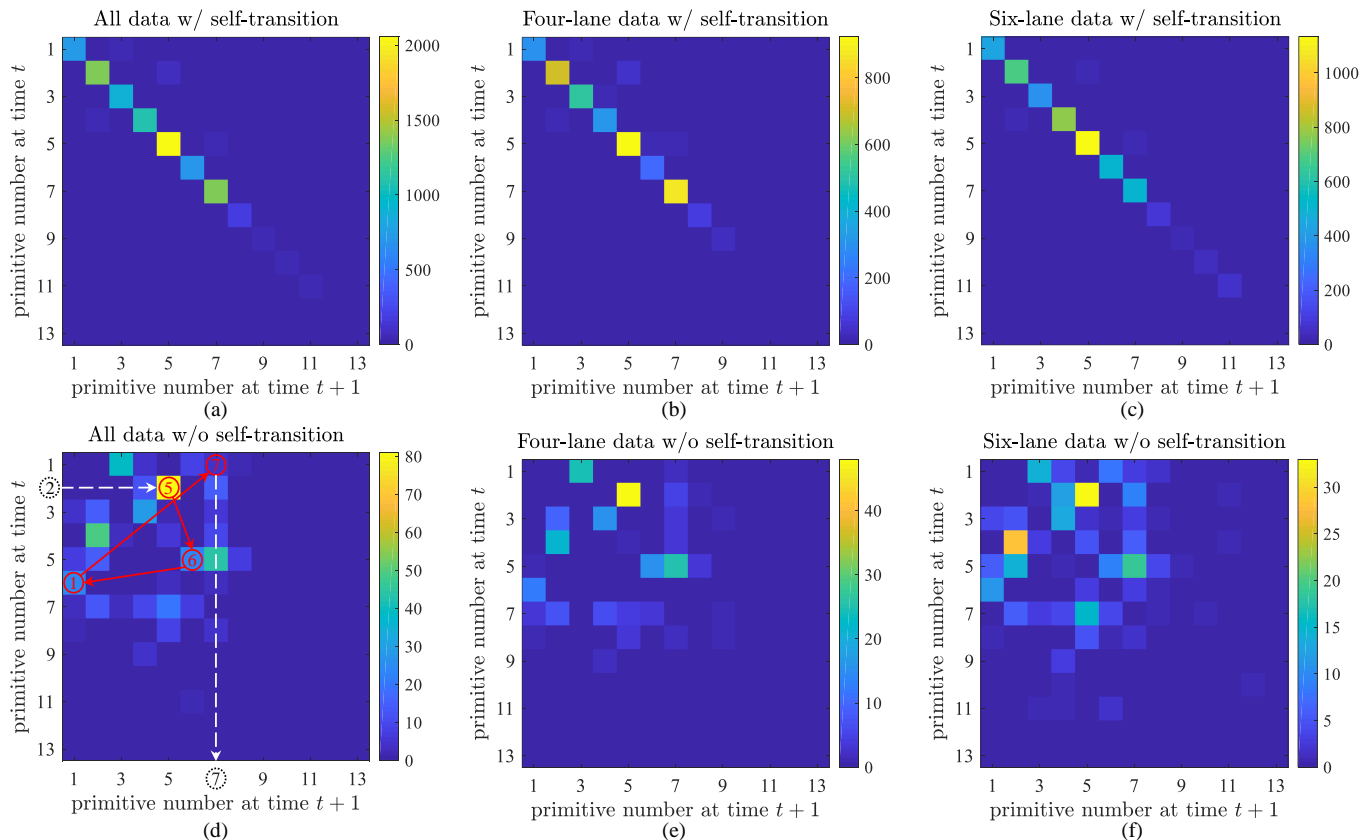


Fig. 15. Transition frequency matrix of the extracted interaction patterns in lane-change region.

The distributions of  $(v_x, a_x)$ ,  $(v_x, a_y)$ ,  $(v_y, a_x)$ , and  $(v_y, a_y)$  for each pattern are detailed in the supplementary materials (see Appendix). Besides, the patterns transition, the renderings of the real-time velocity fields, and the bird’s-eye-view scenarios are all provided in our video demos of 32 cases to help with a better intuition; also see Appendix.

### E. Transitions of Interaction Patterns

The above section discussed the extracted interaction patterns during lane change in a spatial view. In what follows, we will gain an insight into how one interaction pattern switches to another one over time and reveal their causal relationships. Investigating lane-change behavior is usually over several independent stages of the ego vehicle’s maneuvers, such as preparation, execution, and termination, but without considering interactions with other vehicles. In order to uncover how our learned interaction patterns behave in the stages defined by state-of-the-art approaches, we delineate the lane-change trajectory into mainly three stages as in [55]: pre-region, lane-change region, and post-region. Our focus in this paper is mainly on the transition of interaction patterns occurred in the lane-change region, as marked in Fig. 14.

Fig. 15 displays the transition frequency among interaction patterns in different road contextual settings (four-lane and six-lane divided highways, as well as their mixtures) with/without counting the self-transition frequency of patterns. Yellow and blue represent the high and low frequency of transiting

between patterns, respectively. Results indicate that these interaction patterns during the lane-change region distinctly have a higher transition frequency within themselves than that between them. The corresponding analysis results of the other two regions (pre-region and post-region) are reported in the supplementary materials (see Appendix).

Fig. 14 discloses the transition probability of interaction patterns straightforwardly over colored trajectories. For example, the ego vehicle in Fig. 14(a) is cutting into the right lane, thus giving a way to a faster following vehicle on the original lane. The whole interaction process is decomposed into five interaction phases associated with five patterns, noted as a pattern transition chain: #2  $\rightarrow$  #5  $\rightarrow$  #6  $\rightarrow$  #1  $\rightarrow$  #7. More detailed semantic interpretation of each pattern has been given in Section V-D. Correspondingly, Fig. 15(d) presents this pattern transition chain in the transition matrix. The white dashed arrows represent the transition of interaction patterns in the pre-region and post-region, and the red solid arrows represent the transition of interaction patterns in the lane-change region. Noted that this transition matrix in Fig. 15 solely represents the transition frequencies of interaction patterns in the lane-change region, and a part of pattern #2 also occurs in the lane-change region. More dynamic scenarios can be found in our supplementary materials, and the associated transition chains of interaction patterns can also be shown in a transition matrix.

The whole training data in Fig. 15(a) indicates that the most

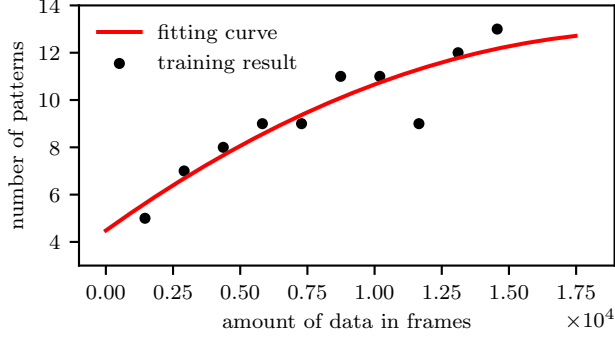


Fig. 16. The obtained number of interaction patterns with different amount of training data.

frequent self-transition pattern is of pattern #5. The most frequent transition between patterns are from pattern #2 to pattern #5 – the beginning of changing lanes from left to right, see Fig. 14(a). The second rank transition frequency is from pattern #4 to pattern #2, in which the ego vehicle changes to the left lane and then overtakes the surrounding vehicle, as illustrated in Fig. 15(c).

In the real-world traffic, it is intuitive for human drivers that changing lanes in a six-lane divided highway scenario is more challenging than that in a four-lane divided highway scenario due to more uncertainties in interacting with surrounding vehicles. Fig. 15 compares the transition frequency of interaction patterns in different road contextual settings: four-lane highways in Fig. 15(b) and (e), and six-lane highways in Fig. 15(c) and (f). Comparisons explicitly tell that the transition matrix in the six-lane divided highway scenario contains more transition patterns than in the four-lane highway scenario. One typical transition is from pattern #4 to pattern #2, as shown in Fig. 15(f).

#### F. Further Discussion

1) *Influence of the size of dataset:* The number of interaction patterns finally learned depends on various factors, such as the size of training data. As we claimed in Section I, the number of interaction patterns, theoretically, should be incrementally increasing as more new scenarios get encountered. This is the critical reason why we implemented the nonparametric model to mimic the increasing number of interactions. Fig. 16 displays the trend in the number of learned interaction patterns when increasing the size of training data, which provides well-matched experimental support for the above claim.

2) *Influence of the ROI definition:* This paper predefined a rectangle area as the ROI and only considered the influence of vehicles in the ROI. A large (small) area of ROI can take more (less) surrounding vehicles into account. For instance, increasing the distance front or behind of the ego vehicle may change the relative velocity field since the vehicles far away from the ego vehicle may fall into the environment and thus would have impacts on velocity field in the ROI. However, our proposed approach is flexible to adapt to other size and shape

of ROI such as polygon [56] because the Gaussian process, theoretically, can describe distributions over infinite functional space in a specific spatial domain.

3) *Potential applications:* Our proposed approach decomposes a long and high-dimensional sequential interaction data into several small interpretable units (i.e., interaction patterns), as displayed in Fig. 14. To some extent, it compresses the complex tasks into efficient, low-dimensional representations that simplify these tasks. Besides, the Bayesian nonparametric models implemented in this paper take clustering, which is a general principle of representation learning [18], i.e., clustering of experience according to similarity for the purposes of delineating task states or patterns. Although the incorporation of such interaction states or patterns into path/trajectory-planning and decision-making algorithms is beyond the focus of this paper, recent techniques have shown how to embed these states or patterns to improve path planning and make more safe decisions, as well as to benefit learning efficiency of algorithms [1], [18], [57]. Further, human driving behaviors cannot be fully understood without the study of the contexts in which behaviors occur [58]; therefore, giving an insight into interactions during lane change can provide detailed prior knowledge with autonomous vehicles to make decisions.

## VI. CONCLUSION

This paper described a nonparametric approach that leverages the continuous and discrete stochastic processes to investigate the underlying interaction of human drivers with their surrounding vehicles, for example, during a lane change on highways. To this end, we first developed a Gaussian velocity field to capture the representation of multi-vehicle interactions over the spatial space while considering the intents of surrounding vehicles. The dimension of the proposed field is insensitive to the number of vehicles in the environment. Besides, we implemented a discrete Bayesian nonparametric model that leverages a hierarchical Dirichlet process and hidden Markov models to learn the interaction patterns over the temporal space. We evaluated the proposed approach based on real-world data with two different traffic contextual settings. Results showed that the proposed nonparametric approach can semantically learn the interaction patterns over the spatiotemporal space for lane change behaviors. Moreover, the proposed approach also reveals the probabilistic transitions among interaction patterns and an explicit understanding of interaction behaviors during lane change, which enables to develop more efficient and safe decision-making policies of lane-change maneuvers for future studies.

## APPENDIX

(a) The distributions of  $(v_x, a_x)$ ,  $(v_x, a_y)$ ,  $(v_y, a_x)$ , and  $(v_y, a_y)$  for all patterns are referred to as the Supplements for “Spatiotemporal Learning of Multivehicle Interaction Patterns in Lane-Change Scenarios”.

(b) The patterns transition, the renderings of the real-time velocity field, and the bird’s-eye-view scenarios of 32 cases are referred to as the link [https://youtu.be/z\\_vf9UHtdAM](https://youtu.be/z_vf9UHtdAM).

(c) The analysis of the transition matrix of the others two regions (pre-region and post-region) are referred to as the Supplements for “Spatiotemporal Learning of Multivehicle Interaction Patterns in Lane-Change Scenarios”.

## REFERENCES

- [1] E. Galceran, A. G. Cunningham, R. M. Eustice, and E. Olson, “Multipolicy decision-making for autonomous driving via changepoint-based behavior prediction: Theory and experiment,” *Autonomous Robots*, vol. 41, no. 6, pp. 1367–1382, 2017.
- [2] C. Zhao, W. Wang, S. Li, and J. Gong, “Influence of cut-in maneuvers for an autonomous car on surrounding drivers: Experiment and analysis,” *IEEE Transactions on Intelligent Transportation Systems*, DOI:10.1109/ITITS.2019.2914795. 2019.
- [3] T. Appenzeller, “The scientist’ apprentice,” *Science*, vol. 357, no. 6346, pp. 16–17, 2017.
- [4] Y. Zhou, M. E. Cholette, A. Bhaskar, and E. Chung, “Optimal vehicle trajectory planning with control constraints and recursive implementation for automated on-ramp merging,” *IEEE Transactions on Intelligent Transportation Systems*, 2018.
- [5] D. Tian, G. Wu, P. Hao, K. Boriboonsomsin, and M. J. Barth, “Connected vehicle-based lane selection assistance application,” *IEEE Transactions on Intelligent Transportation Systems*, 2018.
- [6] W. Schwarting, A. Pierson, J. Alonso-Mora, S. Karaman, and D. Rus, “Social behavior for autonomous vehicles,” *Proceedings of the National Academy of Sciences*, vol. 116, no. 50, pp. 24 972–24 978, 2019.
- [7] D. Kasper, G. Weidl, T. Dang, G. Breuel, A. Tamke, A. Wedel, and W. Rosenstiel, “Object-oriented bayesian networks for detection of lane change maneuvers,” *IEEE Intelligent Transportation Systems Magazine*, vol. 4, no. 3, pp. 19–31, 2012.
- [8] X. Li, W. Wang, and M. Rötting, “Estimating driver’s lane-change intent considering driving style and contextual traffic,” *IEEE Transactions on Intelligent Transportation Systems*, vol. 20, no. 9, pp. 3258 – 3271, 2018.
- [9] M. A. S. Kamal, S. Taguchi, and T. Yoshimura, “Efficient vehicle driving on multi-lane roads using model predictive control under a connected vehicle environment,” in *2015 IEEE Intelligent Vehicles Symposium (IV)*. IEEE, 2015, pp. 736–741.
- [10] Q. H. Do, H. Tehrani, S. Mita, M. Egawa, K. Muto, and K. Yoneda, “Human drivers based active-passive model for automated lane change,” *IEEE Intelligent Transportation Systems Magazine*, vol. 9, no. 1, pp. 42–56, 2017.
- [11] H. Woo, Y. Ji, H. Kono, Y. Tamura, Y. Kuroda, T. Sugano, Y. Yamamoto, A. Yamashita, and H. Asama, “Lane-change detection based on vehicle-trajectory prediction,” *IEEE Robotics and Automation Letters*, vol. 2, no. 2, pp. 1109–1116, 2017.
- [12] S. Yang, W. Wang, C. Lu, J. Gong, and J. Xi, “A time-efficient approach for decision-making style recognition in lane-changing behavior,” *IEEE Transactions on Human-Machine Systems*, vol. 49, no. 6, pp. 579–588, 2019.
- [13] P. Liu, A. Kurt, K. Redmill, and U. Ozguner, “Classification of highway lane change behavior to detect dangerous cut-in maneuvers,” in *The Transportation Research Board (TRB) 95th Annual Meeting*, vol. 2, 2015.
- [14] N. Deo, A. Rangesh, and M. M. Trivedi, “How would surround vehicles move? a unified framework for maneuver classification and motion prediction,” *IEEE Transactions on Intelligent Vehicles*, vol. 3, no. 2, pp. 129–140, 2018.
- [15] L. Claussmann, M. Revilloud, D. Gruyer, and S. Glaser, “A review of motion planning for highway autonomous driving,” *IEEE Transactions on Intelligent Transportation Systems*, 2019.
- [16] M. Guangyu Li, B. Jiang, Z. Che, X. Shi, M. Liu, Y. Meng, J. Ye, and Y. Liu, “Dbus: Human driving behavior understanding system,” in *Proceedings of the IEEE International Conference on Computer Vision Workshops*, 2019, pp. 0–0.
- [17] G. Habibi, N. Japuria, and J. P. How, “Incremental learning of motion primitives for pedestrian trajectory prediction at intersections,” *arXiv preprint arXiv:1911.09476*, 2019.
- [18] Y. Niv, “Learning task-state representations,” *Nature neuroscience*, vol. 22, no. 10, pp. 1544–1553, 2019.
- [19] C. Lienke, C. Wissing, M. Keller, T. Nattermann, and T. Bertram, “Predictive driving: Fusing prediction and planning for automated highway driving,” *IEEE Transactions on Intelligent Vehicles*, vol. 4, no. 3, pp. 456–467, 2019.
- [20] X. Li, W. Wang, Z. Zhang, and M. Rötting, “Effects of feature selection on lane-change maneuver recognition: an analysis of naturalistic driving data,” *Journal of Intelligent and Connected Vehicles*, vol. 1, no. 3, pp. 85–98, 2018.
- [21] V. Leonhardt and G. Wanielik, “Feature evaluation for lane change prediction based on driving situation and driver behavior,” in *2017 20th International Conference on Information Fusion (Fusion)*. IEEE, 2017, pp. 1–7.
- [22] W. Wang and D. Zhao, “Extracting traffic primitives directly from naturalistically logged data for self-driving applications,” *IEEE Robotics and Automation Letters*, vol. 3, no. 2, pp. 1223–1229, 2018.
- [23] Y. Hu, W. Zhan, and M. Tomizuka, “Probabilistic prediction of vehicle semantic intention and motion,” in *2018 IEEE Intelligent Vehicles Symposium (IV)*. IEEE, 2018, pp. 307–313.
- [24] M. T. Wolf and J. W. Burdick, “Artificial potential functions for highway driving with collision avoidance,” in *2008 IEEE International Conference on Robotics and Automation*. IEEE, 2008, pp. 3731–3736.
- [25] H. Wang, Y. Huang, A. Khajepour, Y. Zhang, Y. Rasekhipour, and D. Cao, “Crash mitigation in motion planning for autonomous vehicles,” *IEEE Transactions on Intelligent Transportation Systems*, vol. 20, no. 9, pp. 3313–3323, 2019.
- [26] Y. Rasekhipour, A. Khajepour, S.-K. Chen, and B. Litkouhi, “A potential field-based model predictive path-planning controller for autonomous road vehicles,” *IEEE Transactions on Intelligent Transportation Systems*, vol. 18, no. 5, pp. 1255–1267, 2016.
- [27] H. Woo, Y. Ji, H. Kono, Y. Tamura, Y. Kuroda, T. Sugano, Y. Yamamoto, A. Yamashita, and H. Asama, “Dynamic potential-model-based feature for lane change prediction,” in *2016 IEEE International Conference on Systems, Man, and Cybernetics (SMC)*. IEEE, 2016, pp. 000 838–000 843.
- [28] J. Wang, J. Wu, X. Zheng, D. Ni, and K. Li, “Driving safety field theory modeling and its application in pre-collision warning system,” *Transportation research part C: emerging technologies*, vol. 72, pp. 306–324, 2016.
- [29] W. Wang, J. Xi, and J. K. Hedrick, “A learning-based personalized driver model using bounded generalized gaussian mixture models,” *IEEE Transactions on Vehicular Technology*, vol. 68, no. 12, pp. 11 679–11 690, 2019.
- [30] D. Pelleg, A. W. Moore, *et al.*, “X-means: Extending k-means with efficient estimation of the number of clusters,” in *Icml*, vol. 1, 2000, pp. 727–734.
- [31] C. E. Rasmussen, “The infinite gaussian mixture model,” in *Advances in neural information processing systems*, 2000, pp. 554–560.
- [32] D. Görür and C. E. Rasmussen, “Dirichlet process gaussian mixture models: Choice of the base distribution,” *Journal of Computer Science and Technology*, vol. 25, no. 4, pp. 653–664, 2010.
- [33] E. B. Fox, E. B. Sudderth, M. I. Jordan, and A. S. Willsky, “The sticky hdp-hmm: Bayesian nonparametric hidden markov models with persistent states,” *Arxiv preprint*, 2007.
- [34] N. Raman and S. J. Maybank, “Activity recognition using a supervised non-parametric hierarchical hmm,” *Neurocomputing*, vol. 199, pp. 163–177, 2016.
- [35] M. Jochmann, “Modeling us inflation dynamics: A bayesian nonparametric approach,” *Econometric Reviews*, vol. 34, no. 5, pp. 537–558, 2015.
- [36] R. Hamada, T. Kubo, K. Ikeda, Z. Zhang, T. Shibata, T. Bando, K. Hitomi, and M. Egawa, “Modeling and prediction of driving behaviors using a nonparametric bayesian method with ar models,” *IEEE Transactions on Intelligent Vehicles*, vol. 1, no. 2, pp. 131–138, 2016.
- [37] W. Wang, J. Xi, and D. Zhao, “Driving style analysis using primitive driving patterns with bayesian nonparametric approaches,” *IEEE Transactions on Intelligent Transportation Systems*, vol. 20, no. 8, pp. 2986–2998, 2018.
- [38] H. N. Mahjoub, B. Toghi, and Y. P. Fallah, “A stochastic hybrid framework for driver behavior modeling based on hierarchical dirichlet process,” in *2018 IEEE 88th Vehicular Technology Conference (VTC-Fall)*. IEEE, 2018, pp. 1–5.
- [39] R. J. Bufacchi and G. D. Iannetti, “An action field theory of peripersonal space,” *Trends in cognitive sciences*, 2018.
- [40] C. Zhang, J. Zhu, W. Wang, and D. Zhao, “A general framework of learning multi-vehicle interaction patterns from videos,” in *2019 22nd International Conference on Intelligent Transportation Systems (ITSC)*. IEEE, 2019.
- [41] J. Zhu, S. Qin, W. Wang, and D. Zhao, “Probabilistic trajectory prediction for autonomous vehicles with attentive recurrent neural process,” *arXiv preprint arXiv:1910.08102*, 2019.



- [42] S. Qin, J. Zhu, J. Qin, W. Wang, and D. Zhao, "Recurrent attentive neural process for sequential data," *arXiv preprint arXiv:1910.09323*, 2019.
- [43] C. E. Rasmussen, "Gaussian processes in machine learning," in *Summer School on Machine Learning*. Springer, 2003, pp. 63–71.
- [44] S. Moridpour, E. Mazloumi, and M. Mesbah, "Impact of heavy vehicles on surrounding traffic characteristics," *Journal of advanced transportation*, vol. 49, no. 4, pp. 535–552, 2015.
- [45] A. Ng *et al.*, "Sparse autoencoder," *CS294A Lecture notes*, vol. 72, no. 2011, pp. 1–19, 2011.
- [46] W. Zhang and W. Wang, "Learning v2v interactive driving patterns at signalized intersections," *Transportation Research Part C: Emerging Technologies*, vol. 108, pp. 151–166, 2019.
- [47] N. A. Taatgen, "The nature and transfer of cognitive skills." *Psychological review*, vol. 120, no. 3, p. 439, 2013.
- [48] T. Taniguchi, S. Nagasaka, K. Hitomi, N. P. Chandrasiri, T. Bando, and K. Takenaka, "Sequence prediction of driving behavior using double articulation analyzer," *IEEE Transactions on Systems, Man, and Cybernetics: Systems*, vol. 46, no. 9, pp. 1300–1313, 2015.
- [49] E. B. Fox, E. B. Sudderth, M. I. Jordan, A. S. Willsky, *et al.*, "A sticky hdp-hmm with application to speaker diarization," *The Annals of Applied Statistics*, vol. 5, no. 2A, pp. 1020–1056, 2011.
- [50] Y. W. Teh, M. I. Jordan, M. J. Beal, and D. M. Blei, "Sharing clusters among related groups: Hierarchical dirichlet processes," in *Advances in neural information processing systems*, 2005, pp. 1385–1392.
- [51] M. J. Johnson and A. S. Willsky, "Bayesian nonparametric hidden semi-markov models," *Journal of Machine Learning Research*, vol. 14, pp. 673–701, February 2013.
- [52] R. Krajewski, J. Bock, L. Kloeker, and L. Eckstein, "The highd dataset: A drone dataset of naturalistic vehicle trajectories on german highways for validation of highly automated driving systems," in *2018 IEEE 21st International Conference on Intelligent Transportation Systems (ITSC)*, 2018.
- [53] F. Yan, L. Weber, and A. Luedtke, "Classifying driver's uncertainty about the distance gap at lane changing for developing trustworthy assistance systems," in *2015 IEEE Intelligent Vehicles Symposium (IV)*. IEEE, 2015, pp. 1276–1281.
- [54] T. Dozat, "Incorporating nesterov momentum into adam." 2016.
- [55] W. Yao, H. Zhao, F. Davoine, and H. Zha, "Learning lane change trajectories from on-road driving data," in *2012 IEEE Intelligent Vehicles Symposium*. IEEE, 2012, pp. 885–890.
- [56] M. Schmidt, C. Manna, J. H. Braun, C. Wissing, M. Mohamed, and T. Bertram, "An interaction-aware lane change behavior planner for automated vehicles on highways based on polygon clipping," *IEEE Robotics and Automation Letters*, vol. 4, no. 2, pp. 1876–1883, 2019.
- [57] F. Doshi-Velez, "Bayesian nonparametric approaches for reinforcement learning in partially observable domains," Ph.D. dissertation, Massachusetts Institute of Technology, 2012.
- [58] I. Rahwan, M. Cebrian, N. Obradovich, J. Bongard, J.-F. Bonnefon, C. Breazeal, J. W. Crandall, N. A. Christakis, I. D. Couzin, M. O. Jackson, *et al.*, "Machine behaviour," *Nature*, vol. 568, no. 7753, pp. 477–486, 2019.



**Jiacheng Zhu** is a Ph.D student with the Department of Mechanical Engineering, Carnegie Mellon University. He is interested in building machine learning system that can operate with limited prior knowledge and can adapt to unobserved circumstances. He approaches this goal using probabilistic modeling and approximate inferences. Some of his research topics include (deep) probabilistic graphical models, variational inferences, and traffic scenario recognition.



**Wenshuo Wang** (S'15-M'18) received his Ph.D. degree in Mechanical Engineering from Beijing Institute of Technology, Beijing, China in 2018. Currently, he is a Postdoctoral Researcher at the California Partners for Advanced Transportation Technology (PATH), University of California at Berkeley (UC Berkeley). Before joint UC Berkeley, he has worked as a Postdoctoral Associate at Carnegie Mellon University (CMU) from 2018 – 2019. He also worked as a Research Scholar with UC Berkeley from 2015 – 2017 and with the University of Michigan, Ann Arbor, from 2017 – 2018. His current research focus is on Bayesian nonparametric learning, reinforcement learning on multi-agent interaction behavior modeling and prediction at human-levels for autonomous vehicles, intelligent transportation systems in common-but-challenging situations.



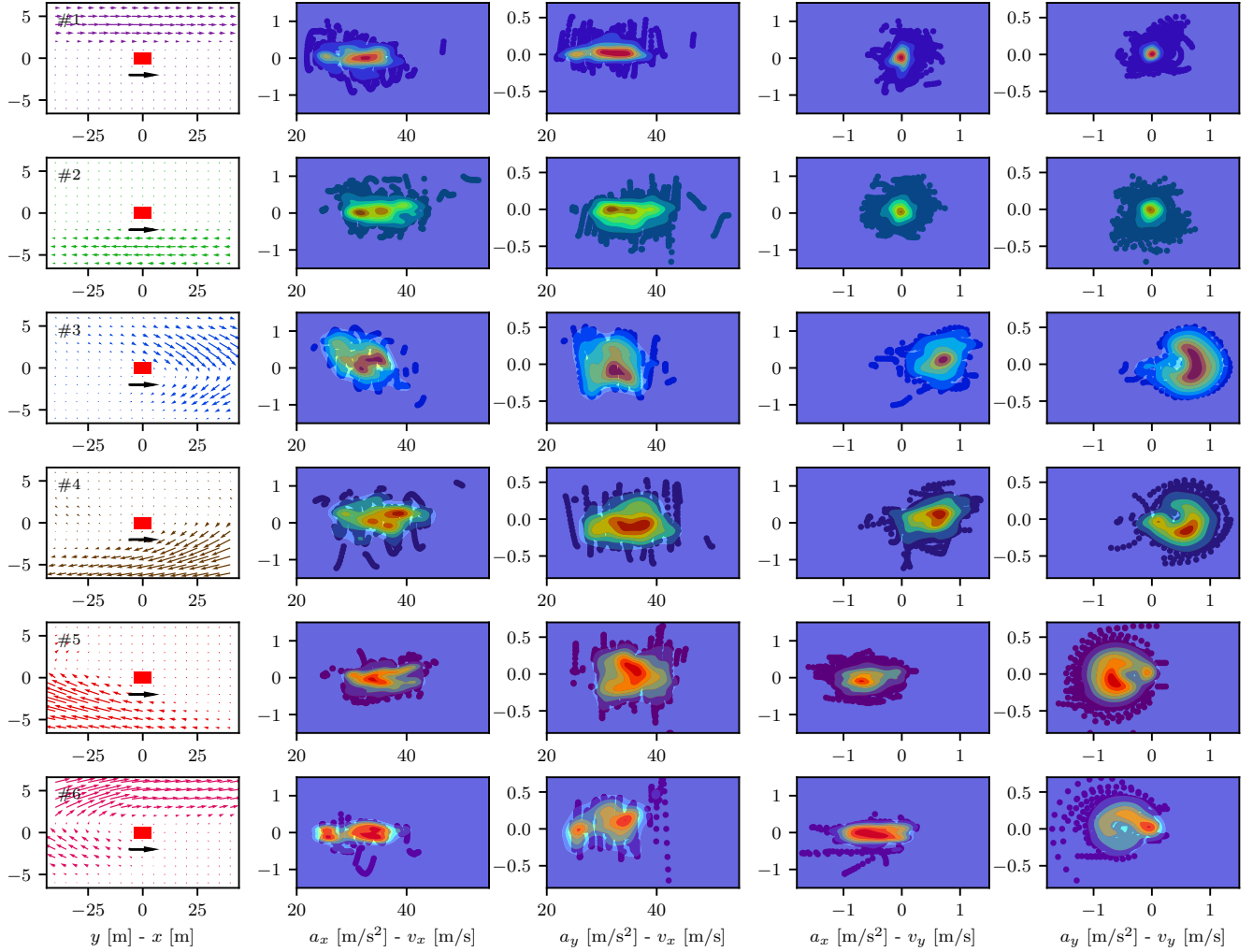
**Junqiang Xi** received the B.S. in Automotive Engineering from Harbin Institute of Technology, Harbin, China, in 1995 and the PhD in Vehicle Engineering from Beijing Institute of Technology (BIT), Beijing, China, in 2001. In 2001, he joined the State Key Laboratory of Vehicle Transmission, BIT. During 2012-2013, he made research as an advanced research scholar in Vehicle Dynamic and Control Laboratory, Ohio State University(OSU), USA. He is Professor and Director of Automotive Research Center in BIT currently. His research interests include vehicle dynamic and control, power-train control, mechanics, intelligent transportation system and intelligent vehicles.



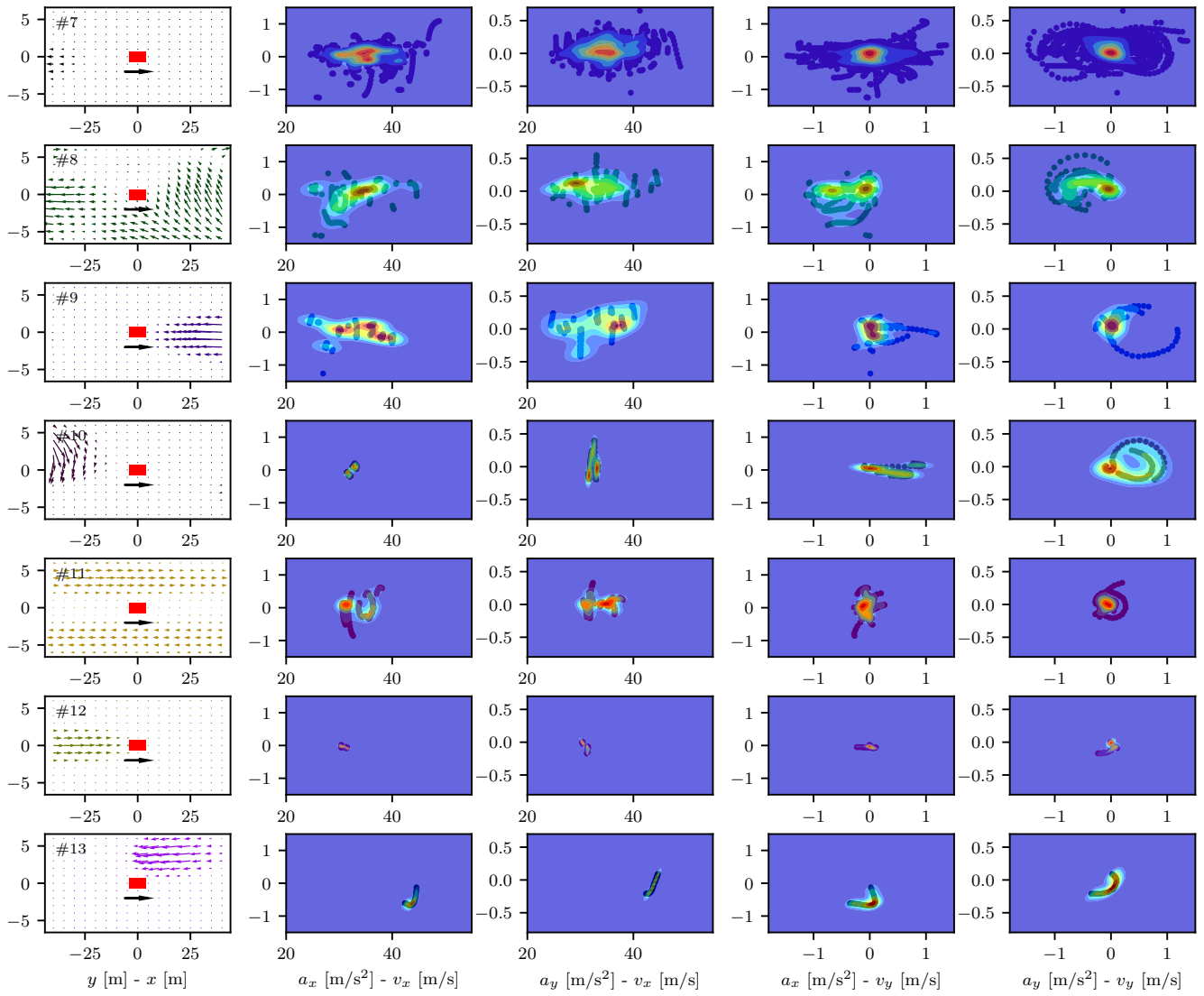
**Chengyuan Zhang** received his B.S. in Automotive Engineering from Chongqing University, Chongqing, China, in 2019. He was a visiting student at the Department of Mechanical Engineering, Carnegie Mellon University, USA, in 2018. Currently, he is a Visiting Student Researcher at the Department of Mechanical Engineering, University of California at Berkeley, USA. His research interests are Bayesian learning, macro/micro driving behavior analysis, intelligent transportation systems, and autonomous vehicle.

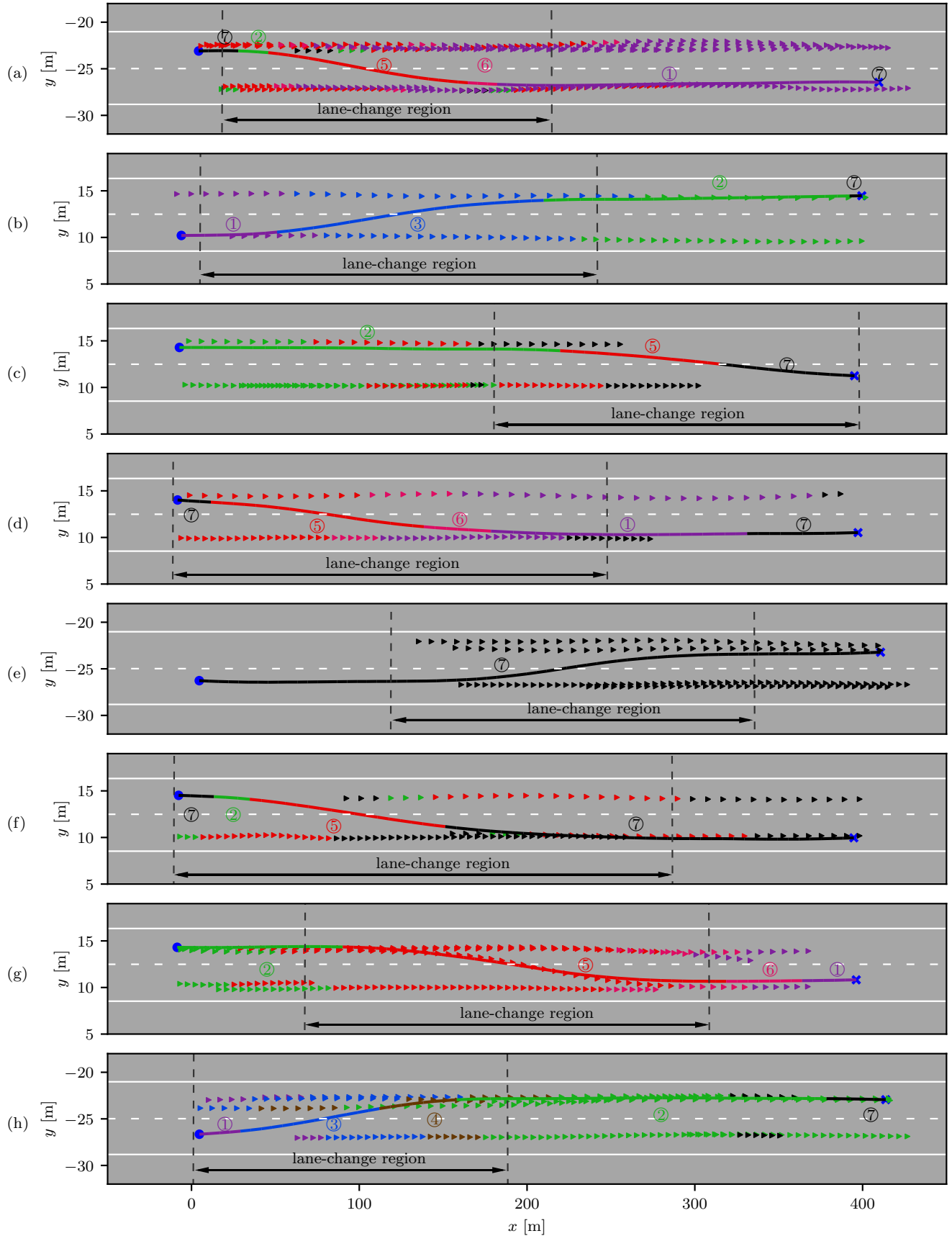
# Supplements for “Spatiotemporal Learning of Multivehicle Interaction Patterns in Lane-Change Scenarios”

Chengyuan Zhang, *Student Member, IEEE*, Jiacheng Zhu, Wenshuo Wang, *Member, IEEE*, Junqiang Xi

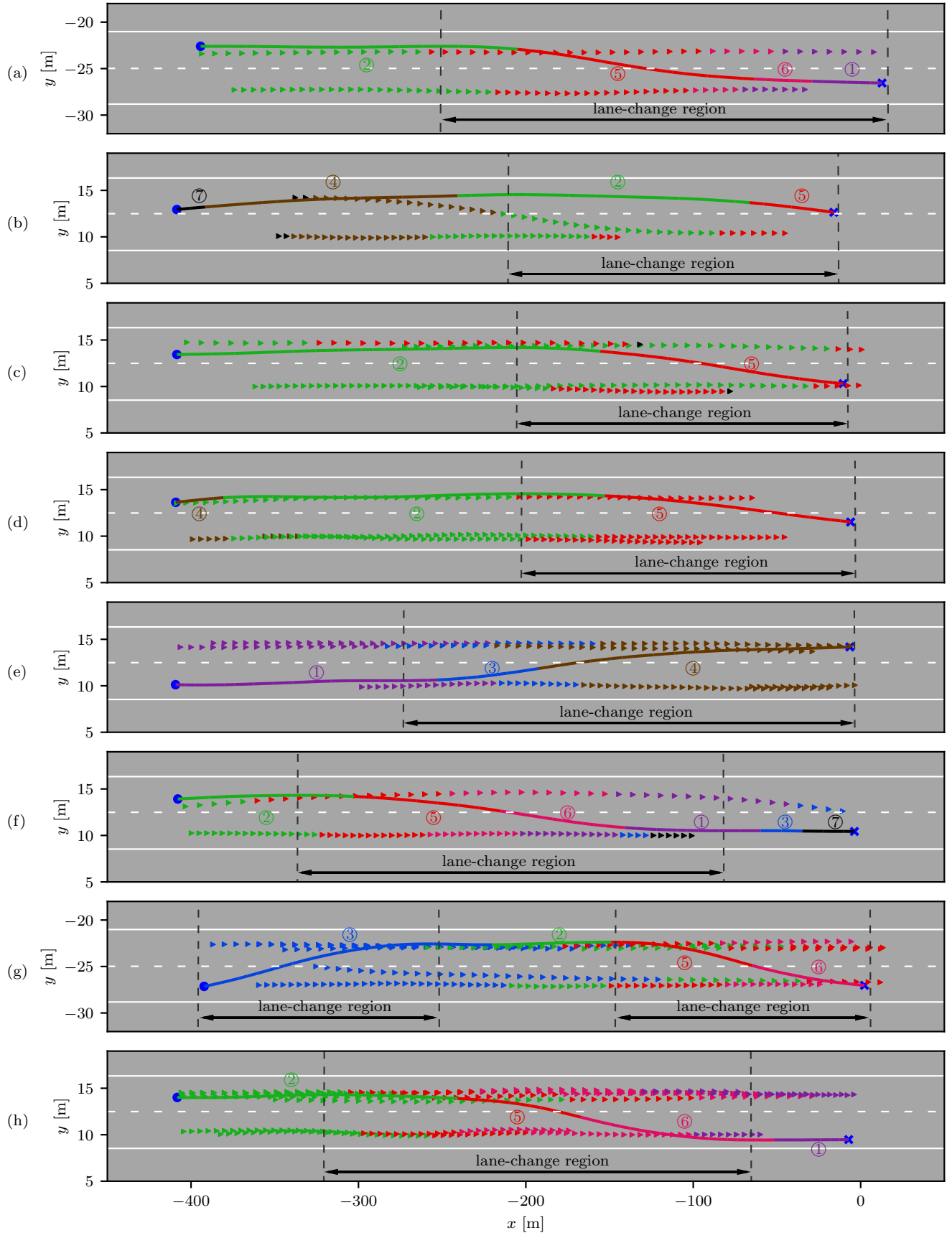


Appendix-Fig. 1: The distributions of  $(v_x, a_x)$ ,  $(v_x, a_y)$ ,  $(v_y, a_x)$ , and  $(v_y, a_y)$  for patterns #1 - #6.



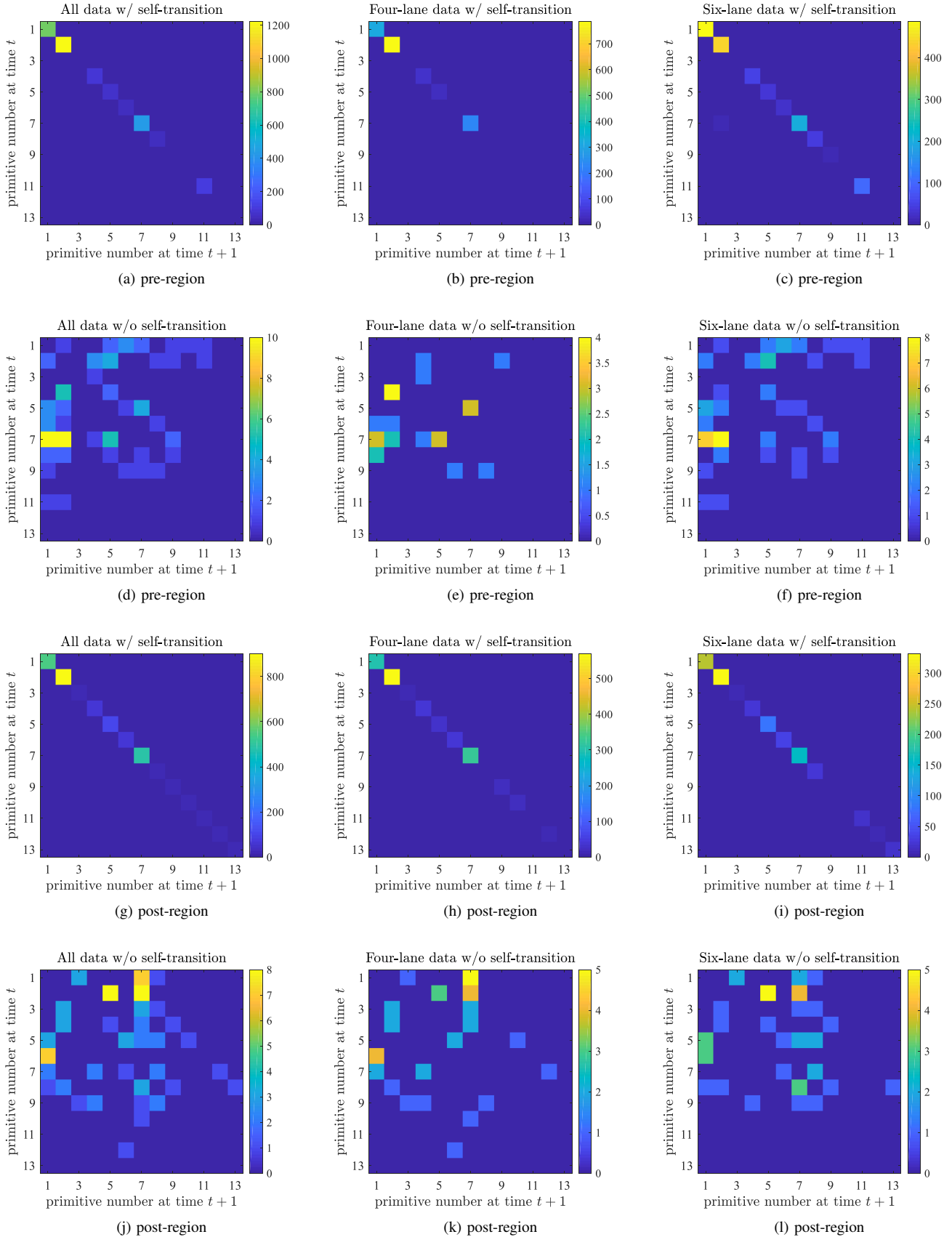


Appendix-Fig. 3: Results of the extracted interaction patterns during lane-change dynamic process.



Appendix-Fig. 4: Results of the extracted interaction patterns during lane-change dynamic process.





Appendix-Fig. 5: Transition probability matrices.